iScience

CellPress
OPEN ACCESS

Article

Enhancing the chondrogenic potential of chondrogenic progenitor cells by deleting RAB5C

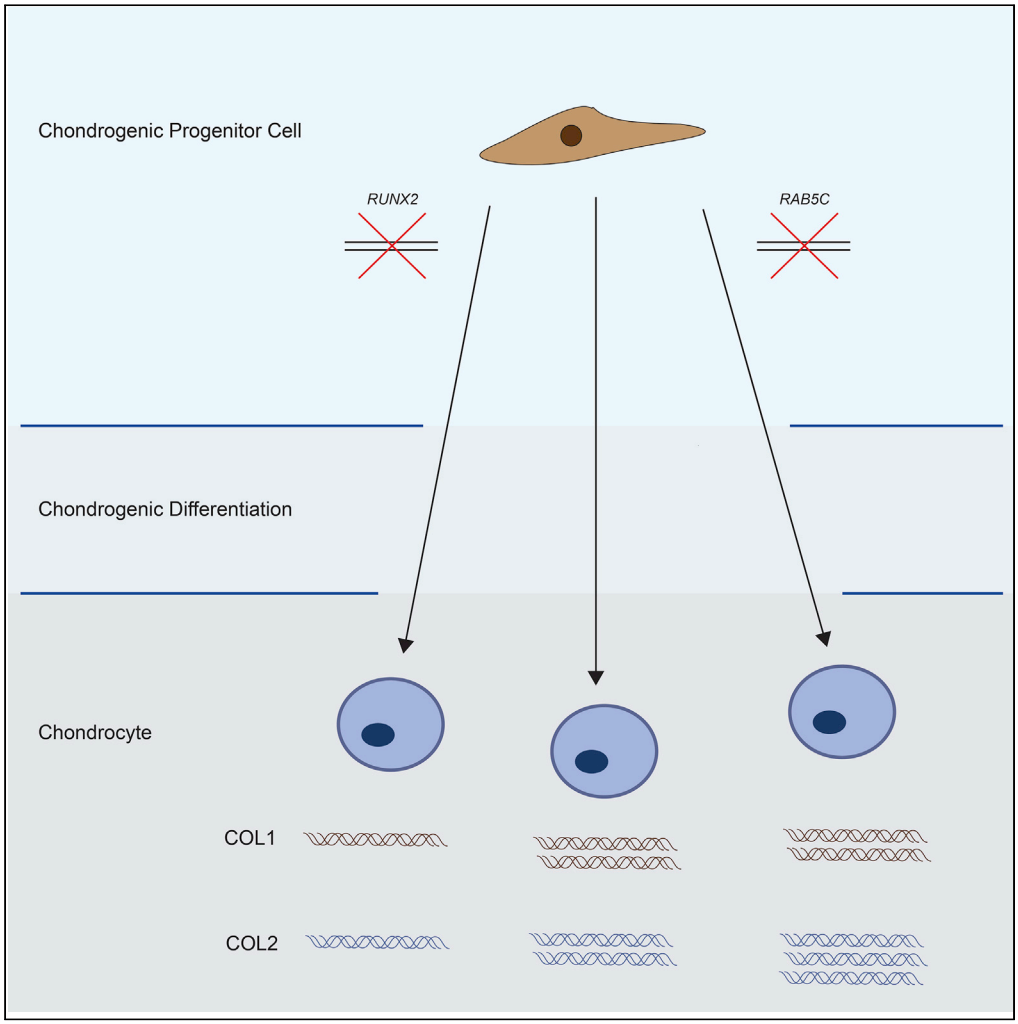

Jerome Nicolas Janssen, Valerio Izzi, Elvira Henze, ..., Christof Lenz, Vicki Rosen, Nicolai Miosge

nmiosge@gwdg.de

Highlights

RUNX2 has a pro-chondrogenic effect in CPCs.

RAB5C is a potential interaction partner of SOX9 in CPCs.

Loss of RAB5C increases the chondrogenic potential of CPCs.

Janssen et al., iScience *24*, 102464
May 21, 2021
https://doi.org/10.1016/j.isci.2021.102464

iScience

CellPress
OPEN ACCESS

Article

Enhancing the chondrogenic potential of chondrogenic progenitor cells by deleting RAB5C

Jerome Nicolas Janssen,[1,5] Valerio Izzi,[2] Elvira Henze,[1] Gökhan Cingöz,[1] Florian Lowen,[1] David Küttner,[1] Ruth Neumann,[1] Christof Lenz,[3,4] Vicki Rosen,[5] and Nicolai Miosge[1,6,*]

SUMMARY

Osteoarthritis (OA) is the most prevalent chronic joint disease that affects a large proportion of the elderly population. Chondrogenic progenitor cells (CPCs) reside in late-stage OA cartilage tissue, producing a fibrocartilaginous extracellular matrix; these cells can be manipulated *in vitro* to deposit proteins of healthy articular cartilage.

CPCs are under the control of SOX9 and RUNX2. In our earlier studies, we showed that a knockdown of RUNX2 enhanced the chondrogenic potential of CPCs. Here we demonstrate that CPCs carrying a knockout of RAB5C, a protein involved in endosomal trafficking, exhibited elevated expression of multiple chondrogenic markers, including the SOX trio, and increased COL2 deposition, whereas no changes in COL1 deposition were observed.

We report RAB5C as an attractive target for future therapeutic approaches designed to increase the COL2 content in the diseased joint.

INTRODUCTION

Osteoarthritis (OA) is the most common musculoskeletal disease in the elderly (Reginster, 2002). According to the WHO, by 2050, 130 million people will suffer from OA and 40 million people will be severely disabled by OA (WHO, 2013). The disease is characterized by the degradation of the articular cartilage, which results in impaired joint functionality (Felson, 2006). Current therapies provide symptomatic relief but are unable to cure the disease, and patients eventually require total joint replacement (Lohmander and Roos, 2007). The search for new OA treatment options focuses on regenerative cell therapies, among others modalities (Brittberg et al., 1994; Schminke and Miosge, 2014).

In the joint, chondrocytes populate the healthy articular cartilage, secreting extracellular matrix (ECM) components such as collagen type II (COL2) and other characteristic proteins that are responsible for the unique properties of the tissue (Buckwalter and Mankin, 1998; Oldberg et al., 1990). During OA, disturbed cell-matrix interactions lead to the degradation of the healthy articular cartilage (Sandell and Aigner, 2001; Poole, 1997; Goldring and Goldring, 2007; Heinegard and Saxne, 2011), resulting in fibrillation processes and the formation of a fibrocartilaginous repair tissue (Miosge et al., 1998, 2004; Horton et al., 2006) that is mainly composed of collagen type I (COL1). This repair tissue lacks the mechanical properties of healthy cartilage (Setton et al., 1999).

Previous studies by our group and others reported that fibrocartilage repair tissue is derived from a unique cell population of migratory, clonogenic and multipotent chondrogenic progenitor cells (CPCs) (Koelling et al., 2009; Seol et al., 2012). *In vitro* experiments have revealed the capacity of CPCs to differentiate into chondrocytes (Joos et al., 2013; Jenei-Lanzl et al., 2014; Embree et al., 2016; Janssen et al., 2019; Wang et al., 2019). Based on these findings, our approach is to increase the chondrogenic potential of CPCs *in vivo*. The differentiation of CPCs is mainly determined by the chondrogenic transcription factor SOX9 and by the osteogenic factor RUNX2 (Koelling et al., 2009). SOX9 is an essential factor expressed throughout the chondrocyte lineage, from mesenchymal chondroprogenitor condensation until hypertrophic differentiation (Bi et al., 1999, 2001), and it regulates the expression of chondrogenic markers such as COL2 (Lefebvre et al., 1997). RUNX2, the master regulator of osteogenesis (Otto et al., 1997), also plays a crucial role in early chondrogenesis. Nullizygous RUNX2 mice exhibit delayed or absent chondrocyte hypertrophy (Kim et al., 1999; Inada et al., 1999). Knockdown of *RUNX2* in CPCs increases the expression of *SOX9*, *ACAN* and *COL2*, but decreases the expression of catabolic markers such as *MMP13* and

[1]Tissue Regeneration Work Group, Department of Prosthodontics, Medical Faculty, Georg-August-University, 37075 Göttingen, Germany

[2]Faculty of Biochemistry and Molecular Medicine, University of Oulu, 90014 Oulu, Finland

[3]Bioanalytical Mass Spectrometry Group, Max Planck Institute for Biophysical Chemistry, 37077 Göttingen, Germany

[4]Institute of Clinical Chemistry, Medical Faculty, Georg-August-University, 37075 Göttingen, Germany

[5]Developmental Biology, Harvard School of Dental Medicine, Boston, MA 02115, USA

[6]Lead contact

*Correspondence: nmiosge@gwdg.de

https://doi.org/10.1016/j.isci.2021.102464

ADAMTS5 (Koelling et al., 2009). Due to the critical and versatile functions of SOX9 (Jo et al., 2014) and RUNX2 (Pratap et al., 2011), we strove for a subtler manipulation of the chondrogenic potential than the direct targeting of these master regulators.

In our study, we identified a pivotal role for RUNX2 in determining the chondrogenic potential of CPCs, and we identified RAB5C as a potential interaction partner of SOX9. By knocking out RAB5C, we increased the chondrogenic potential of CPCs *in vitro* and transplanted these manipulated cells into a nude mice model to analyze its effect *in vivo*. Additionally, we provided the first insights into the possible underlying cell biological mechanism.

RESULTS

Primary and immortalized CPCs did not exhibit major differences

CPCs have been a useful model to study the molecular mechanisms related to the pathology of OA (Seol et al., 2012; Joos et al., 2013; Wang et al., 2020; Matta et al., 2019). First, we wanted to determine whether the immortalized CPCs utilized in our previous studies (Janssen et al., 2019; Wagner et al., 2019) and used here differ from primary CPCs after chondrogenic differentiation. Therefore, we performed proteome profiling using data-independent acquisition mass spectrometry (DIA-MS) to elucidate the differences between the two corresponding CPC cell lines before and after immortalization. Additionally, we included one primary cell line and one immortalized cell line from a different patient to consider the effects related to different patient origins. After the chondrogenic differentiation of these cell lines, the DIA-MS analysis detected 2449 proteins. Only 43 proteins (1.76%) in the two corresponding cell lines and 20 proteins (0.82%) in the non-matching cell lines were downregulated after immortalization (Figure S1A and Table S1). Only 16 proteins (0.65%) were upregulated in both corresponding cell lines after immortalization, while only 33 proteins (1.35%) were upregulated in the non-matching cell lines (Figure S1B). Further analysis of these deregulated proteins revealed no significant enrichment of terms related to chondrogenesis. For detailed results see Figure S1C and Table S2.

Therefore, we concluded that immortalization did not substantially deregulate the proteome, thus confirming that our immortalized cell lines, one of which was used in the following experiments, represent a suitable model to investigate the mechanisms of OA and the role of CPCs in chondrogenic regeneration.

The osteogenic master regulator RUNX2 has a pro-chondrogenic function in CPCs

As described in previous studies, CPCs reside in the fibrocartilaginous repair tissue of patients with late-stage OA (Miosge et al., 1998) and can be manipulated *in vitro* to produce hyaline cartilage proteins (Koelling et al., 2009; Dai et al., 2020). Because CPCs are controlled by the osteogenic regulator RUNX2 and the chondrogenic regulator SOX9, diminished *RUNX2* expression induced by RNA interference led to upregulation of the articular cartilage marker *COL2* and downregulation of the fibrocartilaginous marker *COL1* (Koelling et al., 2009). Thus, we were interested in determining whether we would be able to further enhance this effect by knocking out *RUNX2* using a CRISPR/Cas9 approach targeting exon 2 (Figure 1A). First, the $CPC^{RUNX2-/-}$ cell line was examined in 2D culture, and the successful deletion of this exon was confirmed using PCR (Figure 1B). Decreased *SOX9* and *RUNX2* expressions (Figure 1C) were detected using qPCR. Subsequently, an unchanged level of the SOX9 protein and the complete absence of the RUNX2 protein were demonstrated by Western Blot (Figure 1D).

In the next step, $CPC^{Control}$ and $CPC^{RUNX2-/-}$ were cultivated in 3D alginate for 28 days to induce chondrogenic differentiation. No significant changes in *SOX9*, *COL1A1*, and *COL2A1* expression were detected (Figure 1E). Regarding the protein level, we did not observe a change in the SOX9 level, whereas the levels of COL1 and particularly COL2 were substantially decreased (Figure 1F). We propose that a minimal amount of RUNX2 is required to enhance the chondrogenic potential of CPCs, and therefore we anticipated decreased but not abolished RUNX2 levels in subsequent experiments.

In consideration of future therapeutic approaches, strategies directly targeting RUNX2 or SOX9 might have severe consequences due to their numerous upstream functions in various cell types (Valenti et al., 2016; Pritchett et al., 2011; Izzi et al., 2019; Hanley et al., 2008). Furthermore, testing of CPCs carrying a knockout of candidate genes reported in the literature and known to be involved in the pathogenesis of arthritis, namely, *MFGE8* (Albus et al., 2016) and *YWHAE* (Nefla et al., 2015), did not improve chondrogenic

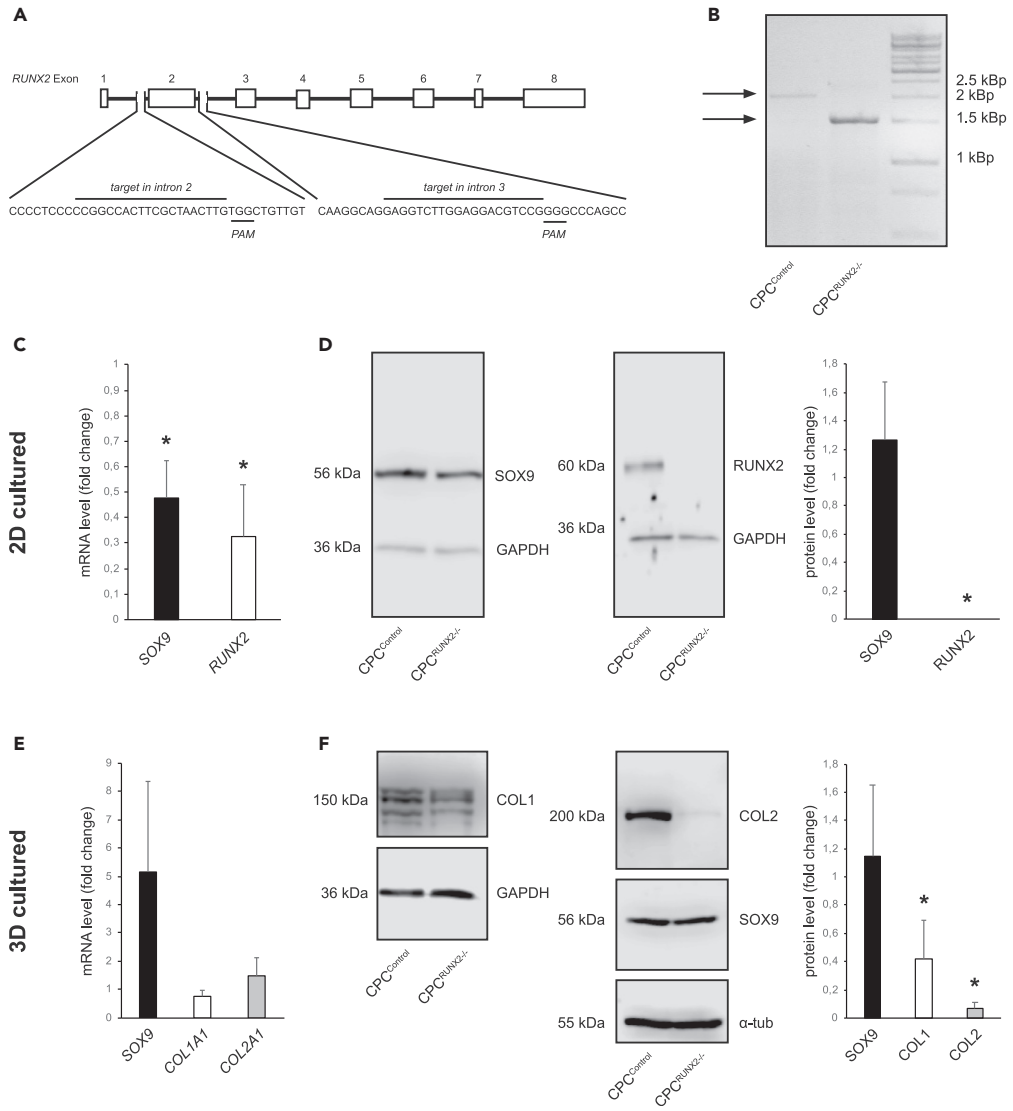

Figure 1. Generation and characterization of CPC$^{RUNX2-/-}$

(A) Schematic of the *RUNX2* locus. Exon lengths are scaled, while intron sizes are reduced for better visualization.
(B) PCR analysis of the *RUNX2* exon 2 locus showing the deletion of 500bp in CPC$^{RUNX2-/-}$ by CRISPR/Cas9.
(C) qPCR analyses of *SOX9* (n = 3) and *RUNX2* (n = 3).
(D–F)(D) Western blot analyses of SOX9 (n = 3) and RUNX2 (n = 3) levels in 2D cultured CPC$^{RUNX2-/-}$. 3D cultured CPC^{Control} and CPC$^{RUNX2-/-}$ were subjected to (E) qPCR analyses of *SOX9* (n = 3), *RUNX2* (n = 4), *COL1* (n = 5) and *COL2* (n = 4), and (F) Western blot analyses of SOX9 (n = 4), COL1 (n = 6, all bands were measured) and COL2 (n = 3) levels.
Abbreviations: PAM, protospacer adjacent motif. Graphs C-F represent means ± SD. Student's t-test, *p < 0.05.

differentiation *in vitro* (data not shown). Therefore, we aimed to identify potential interaction partners of SOX9 whose manipulation might enhance the chondrogenic potential of CPCs.

Loss of RAB5C increases COL2 synthesis in CPCs

For the next approach, we assumed that proteins influencing the chondrogenic potential of CPCs directly or indirectly interact with SOX9 and thus would be identified by a SOX9-His pulldown. First, the SOX9 bait protein was produced in HEK293T cells transfected with pPM-hSOX9His (Figure 2A). For the pulldown, non-specific binding of proteins was assessed by using a column without the SOX9 bait and CPC^{Control} lysate (Figure 2B left lane, for full blot see Figure S2). For the detection of specifically binding proteins, we assumed that an increased SOX9 level promotes the expression of proteins related to chondrogenesis

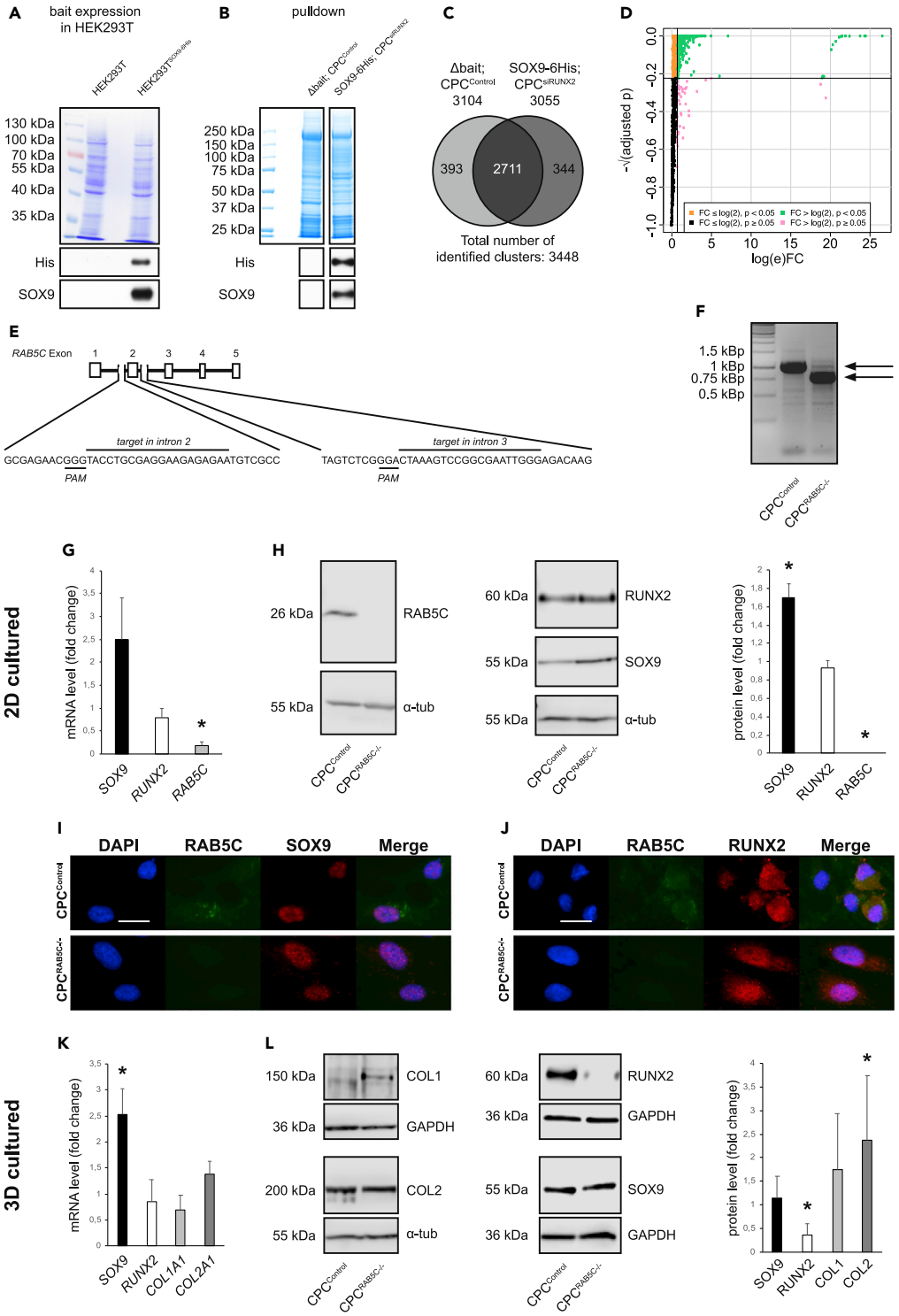

Figure 2. Pulldown of SOX9-associated proteins and characterization of CPC$^{RAB5C-/-}$

(A) Coomassie staining of the lysates of control or SOX9-6His-transfected HEK293T cells. The His tag and SOX9 were detected using Western blotting.

(B) Coomassie-stained SDS gel of control and CPC^{siRUNX2} eluates after Δbait or SOX9-His pulldown. The His tag and SOX9 were detected using Western blotting.

(C) Overview of proteins detected in CPC^{Control} and CPC^{siRUNX2} using mass spectrometry.

Figure 2. *Continued*

(D) Volcano plot of the identified relevant proteins in $CPC^{siRUNX2}$ compared to $CPC^{Control}$.
(E) Schematic of the *RAB5C* locus with scaled exons and reduced intron sizes for better visualization.
(F) CRISPR/Cas9-mediated deletion of 250 bp of *RAB5C* exon 2 was confirmed by PCR.
(G) qPCR analyses of *SOX9* (n = 5), *RUNX2* (n = 5) and *RAB5C* (n = 5) expression in 2D cultured $CPC^{RAB5C-/-}$.
(H–J)(H) Western blotting of SOX9 (n = 3), RUNX2 (n = 3) and RAB5C (n = 3). ICC staining of $CPC^{Control}$ and $CPC^{RAB5C-/-}$ for DAPI, RAB5C and (I) SOX9 or (J) RUNX2. Scale bar: 20 μm. $CPCs^{RAB5C-/-}$ were cultured in 3D alginate for 28 days.
(K and L)(K) qPCR analyses of *SOX9* (n = 5), *RUNX2* (n = 5), *COL1* (n = 5) and COL2 (n = 4) expression, and (L) Western blotting of SOX9 (n= 7) RUNX2 (n = 6), COL1 (n = 6, all bands were measured) and COL2 (n = 7) levels of 3D cultured $CPC^{Control}$ and $CPC^{RAB5C-/-}$. Abbreviations: His, polyhistidine tag; PAM, protospacer adjacent motif. Graphs G, H, K, L represent means ± SD. Student's t-test, *$p < 0.05$.

in CPCs. Therefore, we used the lysate of $CPC^{siRUNX2}$ expressing increased levels of SOX9 (Koelling et al., 2009) to increase the efficiency of the pulldown (Figure 2B, right lane). For control, aliquots of the lysate were run on an SDS gel and used for Western Blot to detect SOX9 and the His-tag. The mass spectrometry analysis revealed 3448 identified protein clusters with 393 protein clusters identified exclusively in the control, while 344 clusters were exclusively related to $CPC^{siRUNX2}$ (Figure 2C). The statistical analysis revealed a number of significantly enriched proteins (Figure 2D). SOX9, which has been described to form homodimers (Huang et al., 2015), was among the 50 most enriched proteins (Table 1). Furthermore, three different RAB proteins involved in vesicular trafficking were detected. One of these proteins, RAB23 was investigated in the mouse ATDC5 cell line, however the manipulation of this protein decreases SOX9 levels (Yang et al., 2008). The other candidate RAB2A has not been linked to chondrogenesis before. Therefore, we decided to analyze RAB5C, an early endosomal marker that already has been linked to EGF signaling (Miaczynska et al., 2004), which participates in the chondrogenesis of CPCs (Janssen et al., 2019).

First, we generated a $CPC^{RAB5C-/-}$ line by targeting the flanking introns of *RAB5C* exon 2 using CRISPR/Cas9 (Figure 2E), as confirmed by PCR (Figure 2F). An analysis of 2D cultured $CPC^{RAB5C-/-}$ did not reveal significant changes in *SOX9* and *RUNX2* expression, but *RAB5C* expression was reduced (Figure 2G). Subsequently, successful depletion of the RAB5C protein, an increased level of the SOX9 protein and an unchanged level of RUNX2 protein were observed using western blot (Figure 2H). As RAB5C was identified using the SOX9-His pulldown, *in vitro* co-localization of SOX9 and RAB5C was investigated with the help of immunocytochemistry (ICC). SOX9-RAB5C co-localization was not observed in the control, as SOX9 staining was mainly detected in the nucleus, marked by 4',6-diamin-2-phenylinol (DAPI) (Figure 2I). Furthermore, the deletion of RAB5C did not alter the nuclear localization of SOX9. The lysosomal degradation of RUNX2 is promoted by SOX9 (Cheng and Genever, 2010); therefore, we assessed the co-localization of RUNX2 with the early endosomal marker RAB5C (Figure 2J). Co-localization was observed in the cytoplasm of $CPC^{Control}$, but the deletion of RAB5C did not alter the localization of RUNX2. Subsequently, we performed an *ex vivo* migration experiment to determine whether the loss of RAB5C prevents CPCs from migrating into late-stage OA cartilage tissue, a key feature of manipulated CPCs in future therapeutic interventions. Therefore, $CPC^{Control}$ and $CPC^{RAB5C-/-}$ were transfected with GFP and placed on the surface of the OA repair tissue. After 4 days, GFP-positive $CPC^{Control}$ and $CPC^{RAB5C-/-}$ were observed at a depth of approximately 1800 μm in the OA tissue specimens, indicating that the loss of RAB5C did not affect the migratory potential of CPCs (Figure S3).

In order to elucidate changes in the chondrogenic potential, $CPC^{Control}$ and $CPC^{RAB5C-/-}$ underwent chondrogenic differentiation in 3D alginate culture for 28 days. We confirmed a significant increase in *SOX9* expression, but the expression of *COL1A1* and *COL2A1* remained unchanged (Figure 2K). Moreover, the level of the RUNX2 protein was decreased (Figure 2L). Because the level of the COL2 protein increased, $CPC^{RAB5C-/-}$ passed the first hallmark of our screen for candidates for a potential therapeutic intervention to ameliorate OA pathogenesis in the future.

Loss of RAB5C did not impede proliferation and ECM deposition by CPC in a nude mouse model

We were interested to observe if $CPC^{RAB5C-/-}$ exhibited signs of impaired vitality or ECM synthesis under conditions resembling an *in situ* environment. Therefore, we performed a nude mice experiment to check the occurrence of essential marker proteins by qualitative immunohistochemical (IHC) staining. Alginate beads containing $CPC^{Control}$ or $CPC^{RAB5C-/-}$ and empty alginate beads serving as a negative control were transplanted into skin pockets of nude mice. After 28 days of nourishment of the cells in the beads

Table 1. Top50 proteins identified by SOX9-His pulldown

Protein name	log(2)FC (SOX9-6His, $CPC^{siRUNX2}$/Δbait, $CPC^{Control}$)	adjusted p
MX2	26.59	5.26×10^{-131}
GDN	24.49	1.23×10^{-16}
PAR14	24.36	1.07×10^{-38}
ISG15	23.79	2.84×10^{-22}
CFA20	21.95	3.93E-10
DOC11	21.51	6.65×10^{-7}
SPTC3	21.51	6.65×10^{-7}
SAP18	21.23	1.85×10^{-5}
NRDC	21.16	3.55×10^{-5}
SI1L2	20.74	8.31×10^{-4}
RAB23	20.35	2.16×10^{-3}
NU214	20.16	5.22×10^{-3}
SOX9	7.14	1.19×10^{-6}
KRT85	6.06	4.53×10^{-2}
LAMB2	4.99	4.96×10^{-42}
DDX60	4.27	5.82×10^{-97}
OASL	4.13	2.14×10^{-17}
MAP1A	3.88	2.24×10^{-13}
NOTCH2	3.77	6.30×10^{-12}
FAT1	3.62	3.13E-10
CNTP1	3.53	2.28×10^{-3}
OAS2	3.47	7.97×10^{-9}
STING	3.23	6.98×10^{-7}
TB10A	3.23	6.98×10^{-7}
LAMB1	3.06	7.66×10^{-35}
RAB2A	3.05	8.57×10^{-6}
MKRN2	2.90	5.37×10^{-5}
RASK	2.90	7.16×10^{-9}
KRT84	2.82	3.57×10^{-2}
GP124	2.78	1.09×10^{-3}
*NEO*1	2.68	5.29×10^{-7}
AGRIN	2.67	1.22×10^{-27}
CAV1	2.57	2.92×10^{-6}
QSOX1	2.49	2.46E-10
FINC	2.49	5.20×10^{-8}
DDX6L	2.49	7.69×10^{-67}
EI2BE	2.47	4.37E-10
BACH	2.41	3.33×10^{-5}
PRDBP	2.40	2.73×10^{-6}
DNMT1	2.36	6.92×10^{-5}
ZFPL1	2.36	4.69×10^{-4}
SC11A	2.24	1.48×10^{-2}
SHRM3	2.22	2.24E-20
LAMC1	2.21	3.15×10^{-7}

(*Continued on next page*)

Table 1. *Continued*

Protein name	log(2)FC (SOX9-6His, $CPC^{siRUNX2}$/Δbait, $CPC^{Control}$)	adjusted p
ACBD5	2.20	3.59×10^{-4}
SYNJ2	2.19	7.60×10^{-7}
RAB5C	2.18	3.67×10^{-3}
CP135	2.17	6.55E-10
FGF2	2.13	2.93×10^{-5}
CCPG1	2.12	9.68×10^{-36}

by tissue fluids instead of chondrogenic medium, the beads were retrieved from the mice for further analysis. The alginate chosen led to an immune response of the mouse host despite our careful selection of the product. The fibrous capsule formed is a physical barrier for most of the mouse cells (Figures 3A and 3B, asterisk). Furthermore, the alginate beads do not offer an attractive habitat as such. It is unlikely that an invasion of murine progenitor cells, possibly from the adipose tissue of the skin into the alginate bead occurred. Living and dead cells were observed by HE staining of the alginate beads carrying $CPC^{Control}$ or $CPC^{RAB5C-/-}$ at the time point of implantation (Figure 3B). The formation of chondrocyte clusters was observed in $CPC^{Control}$ (Figure 3C) and $CPC^{RAB5C-/-}$ (Figure 3D). Also, blood vessel formation into the beads was seen (Figure 3E). Subsequently, we examined the cells with IHC (Figure 3F). First, proliferation was assessed using KI-67 staining and revealed proliferating cells, particularly in cell clusters. When the ECM composition was analyzed, $CPC^{RAB5C-/-}$ deposited COL1 and COL2. Furthermore, we also detected positive staining for aggrecan (ACAN), which has a key function in healthy hyaline cartilage (Heinegard and Saxne, 2011).

In conclusion, CPCs were still able to proliferate despite the deletion of RAB5C. Additionally, qualitative IHC staining revealed the deposition of COL2 and ACAN, both of which are abundant in healthy articular cartilage. This finding allowed us to continue with a deeper and quantitative analysis of the $CPC^{RAB5C-/-}$, including additional markers related to the chondrogenesis of CPCs.

Further characterization of $CPC^{RAB5C-/-}$ revealed increased expression of chondrogenic markers

In this step, we investigated the expression of additional chondrogenic markers using RNA-Seq. $CPC^{Control}$ and $CPC^{RAB5C-/-}$ samples were collected on days 0, 3, and 28 of chondrogenic differentiation *in vitro*. Raw data showed good clustering by genotype and differentiation stage (Figures S4A and S4B), and the 100 most variable genes across conditions are shown in Figure S4C. We determined the expression profile of all cartilage-related genes during the onset of the chondrogenic differentiation of $CPC^{Control}$ and $CPC^{RAB5C-/-}$ by performing an enrichment analysis of genes related to the term cartilage morphogenesis using MSigDB (Figure 4A). The initiation of differentiation led to increased enrichment of this signature from day 0 to day 3 in both cell lines ($CPC^{Control}$ and $CPC^{RAB5C-/-}$, $p<0.001$). $CPC^{RAB5C-/-}$ displayed a decreased enrichment of signature genes compared to $CPC^{Control}$ on day 3, although no difference was observed between $CPC^{Control}$ and $CPC^{RAB5C-/-}$ on day 28.

Next, we focused on important cartilage markers. Figures 4B–4D shows all genes that displayed a significant difference in expression between $CPC^{Control}$ and $CPC^{RAB5C-/-}$ at least at one time point. The increased expression of chondrogenic transcription factors and cartilage markers (Figures 4B and 4D) and the decrease in the expression of fibrotic markers (Figure 4C) in $CPC^{Control}$ is consistent with previous studies of 3D alginate cultures (Kumar and Lassar, 2009).

A detailed analysis of the SOX trio (Figure 4B), which plays a major role in chondrogenesis (De Crombrugghe et al., 2001), allowed us to observe higher expression of *SOX5* in $CPC^{RAB5C-/-}$ than in $CPC^{Control}$ at every time point. Next, higher *SOX6* expression was detected in $CPC^{RAB5C-/-}$ on days 0 and 28 than in $CPC^{Control}$. The *SOX9* expression level was elevated in $CPC^{RAB5C-/-}$ every day compared to the respective control, consistent with the results shown in Figure 2K.

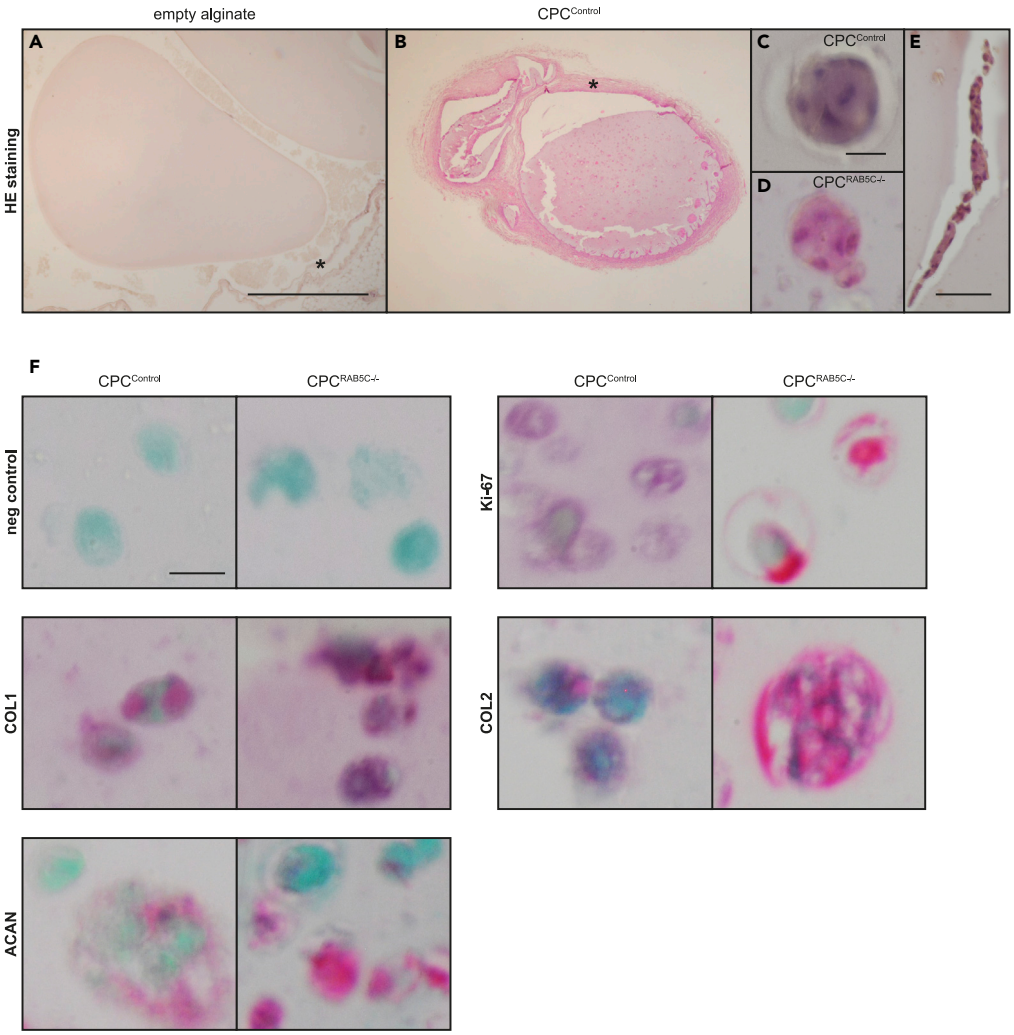

Figure 3. Histological examination of alginate beads transplanted into the back of nude mice

(A) HE staining of implanted beads did not reveal migration of mouse cells into the beads, as evidenced by the empty alginate control and (*) encapsulation of beads.

(B–D)(B) Representative images of HE staining of alginate beads carrying $CPC^{Control}$ cells (scale bar: 1 mm). Chondrocyte clusters were observed in animals injected with (C) $CPC^{Control}$ and (D) $CPC^{RAB5C-/-}$ (scale bar: 12.5 μm).

(E) Blood vessel formation into the beads (scale bar: 50 μm).

(F) Negative control staining, Ki-67, COL1, COL2 and ACAN IHC staining for $CPC^{Control}$ or $CPC^{RAB5C-/-}$ (scale bar: 12.5 μm).

Subsequently, we analyzed the fibrocartilage marker *COL1A1* (Figure 4C) and observed higher expression in $CPC^{RAB5C-/-}$ compared to $CPC^{Control}$ on day 0, but its expression decreased to the levels detected in $CPC^{Control}$ on days 3 and 28, consistent with the results of the qPCR analysis of *COL1A1* on day 28 shown in Figure 2K. Higher *COL1A2* expression was observed on day 0 and day 3 in $CPC^{RAB5C-/-}$, which then decreased on day 28 to the level observed in $CPC^{Control}$.

We then investigated markers of hyaline cartilage (Figure 4D). Unfortunately, *COL2A1* expression was not detected using RNA-Seq. Nevertheless, *COL9A2* and *COL11A1* were examined, as both collagens are related to COL2 regulation and organization through crosslinking (Eyre, 1991; Mendler et al., 1989). *COL9A2* expression was increased on day 3 in $CPC^{RAB5C-/-}$ and COL11A1 expression was decreased on day 28 in $CPC^{RAB5C-/-}$ compared to the respective control. We also observed increased *ACAN* expression in $CPC^{RAB5C-/-}$ on days 3 and 28 compared to the respective control.

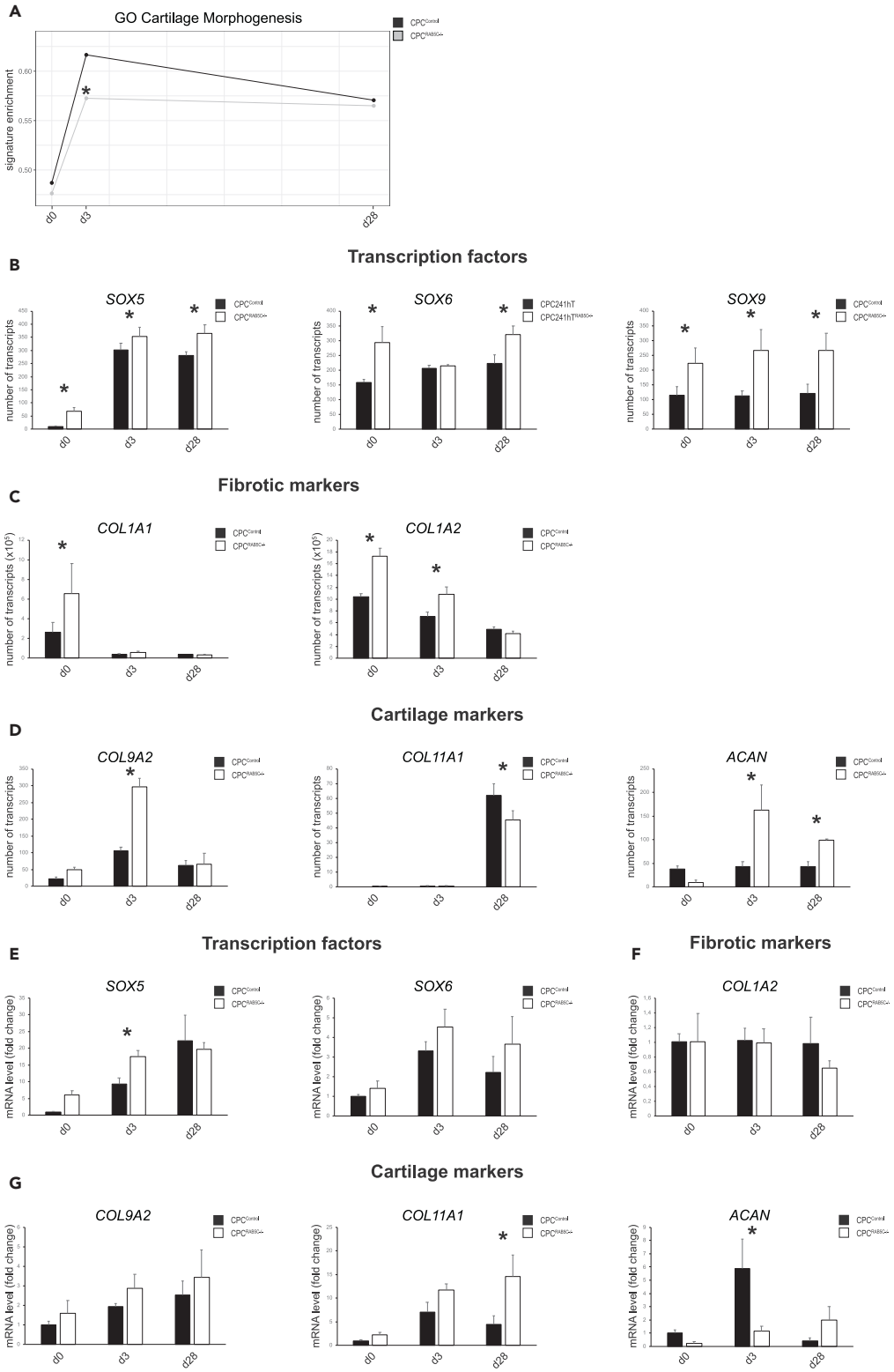

Figure 4. Broader analysis of CPC$^{RAB5C-/-}$ marker expression during chondrogenic differentiation *in vitro*

(A–G)(A) Differential enrichment of genes that are annotated within the category Cartilage Morphogenesis in MSigDB. RNA-Seq analysis of the expression of (B) the transcription factors *SOX5* (n = 3), *SOX6* (n = 3), *SOX9* (n = 3) and *RUNX2* (n = 3), (C) fibrotic markers *COL1A1* (n = 3) and *COL1A2* (n = 3), and (D) cartilage markers *ACAN* (n = 3), *COL9A2* (n = 3) and

Figure 4. *Continued*
COL11A1 (n = 3) in $CPC^{Control}$ and $CPC^{RAB5C-/-}$ on days 0, 3 and 28 of chondrogenic differentiation. qPCR analysis of (E) *SOX5* (n = 5), *SOX6* (n = 5), (F) *COL1A2* (n = 5), (G) *ACAN* (n = 4), *COL9A2* (n = 5) and *COL11A1* (n = 5) expression. Graphs B-G represent means ± SD. Graphs B-D: Mann-Whitney U test with the FDR correction and graphs E-G: ANOVA followed by Tukey's post hoc test, *$p < 0.05$.

We confirmed the results of the RNA-Seq analysis using complementary qPCR (Figures 4E–4G) to further corroborate the higher chondrogenic potential observed after the loss of RAB5C. Consistent with the results presented in Figures 4B and 4D, significantly increased *SOX5* (Figure 4E) and *COL11A1* expression (Figure 4G) were detected at least at one time point in $CPC^{RAB5C-/-}$ compared to $CPC^{Control}$. However, *SOX6* (Figure 4E) and *COL9A2* (Figure 4G) expression were increased in $CPC^{RAB5C-/-}$ at every time point investigated, but the differences were not significant. Finally, differences in *COL1A2* expression were not noticed (Figure 4F), while ACAN expression was increased in $CPC^{Control}$ only on day 3 compared to $CPC^{RAB5C-/-}$(Figure 4G).

Based on these findings, we concluded that the deletion of RAB5C did not lead to severe alterations in the expression of all genes related to chondrogenesis, but it positively affected the expression of the most important chondrogenic markers.

Loss of RAB5C deregulates pathways related to chondrogenesis

We searched for other deregulated genes in $CPC^{RAB5C-/-}$ to find candidates that mediate the observed increase in the chondrogenic potential. Thus, we applied a statistical model based on the hypothesis that the expression of genes related to chondrogenesis will be linear during the course of chondrogenic differentiation. We matched those genes with linear expression in $CPC^{Control}$, but not in $CPC^{RAB5C-/-}$, to identify genes with a possible activating or inhibitory effect on chondrogenesis that are deregulated after the loss of RAB5C (Figure 5A and Table S3). Two members of the BMP signaling pathway, *BMPR1B* and *SMAD7*, fit the model in $CPC^{Control}$, but not in $CPC^{RAB5C-/-}$. Furthermore, *NOTCH3* and *IL4R* were deregulated in $CPC^{RAB5C-/-}$. The qPCR analysis confirmed the lower expression levels of *BMPR1B* on days 3 and 28, *IL4R* on day 3 and *NOTCH3* on day 28, but we did not corroborate our finding for *SMAD7* using qPCR (Figure 5B).

In addition, regarding our *IL4R* results, we performed a GSEA of all deregulated genes in $CPC^{RAB5C-/-}$. The analysis of Gene Ontology and Kyoto Encyclopedia of Genes and Genomes pathway terms revealed a substantial downregulation of genes related to the chemokine signaling pathway, response to chemokine and cytokine–cytokine receptor interaction (Figure S5 and Table S4) including other *IL(R)*s expressed in $CPC^{RAB5C-/-}$on days 3 and 28 of chondrogenic differentiation.

We identified mediators of pathways involved in chondrogenesis that were deregulated at least at one of the time points, and the roles of these proteins should be investigated in future studies to further elucidate the pro-chondrogenic effect observed on $CPC^{RAB5C-/-}$.

In conclusion, an increase of the chondrogenic potential of CPCs is not achieved by the complete deletion of RUNX2. We identified RAB5C as a potential interaction partner of SOX9. RAB5C-deficient CPCs exhibited an increased chondrogenic potential *in vitro* and were capable of producing cartilage markers *in vivo*. An abolishment of COL1 synthesis in CPCs to promote COL2 synthesis is not achieved by the simple upregulation of chondrogenic transcription factors. The effects of the deletion of RAB5C are likely based on altered BMP, Notch, and IL signaling events, rather than direct interactions between SOX9 and RAB5C.

DISCUSSION

A minimal amount of RUNX2 enhances the chondrogenic differentiation of CPCs

Several studies elucidated the essential roles of SOX9 in chondrogenic differentiation and cartilage development (Bi et al., 1999), while studies on the chondrogenic function of RUNX2 have mainly focused on its role in endochondral ossification by inducing chondrocyte hypertrophy (Inada et al., 1999). Our previous study reported the enhanced chondrogenic potential of $CPC^{siRUNX2}$ (Koelling et al., 2009), but here we observed that the total absence of RUNX2 negatively affects COL2 synthesis, while the level of SOX9, a strong activator of COL2, remained unchanged. The assumption that RUNX2 positively

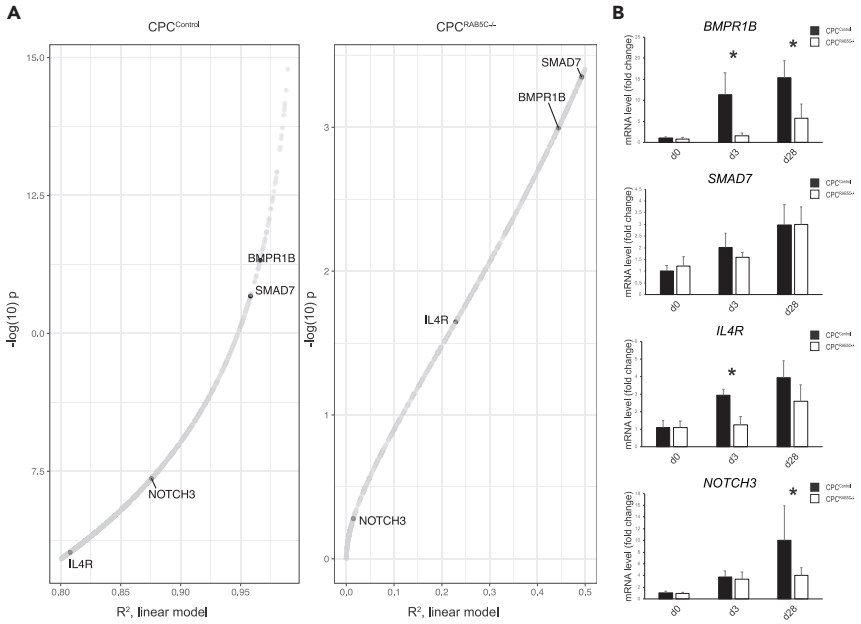

Figure 5. Differential expression of mediators involved in chondrogenesis in CPC$^{RAB5C-/-}$

(A) Analysis of genes identified by RNA-Seq fitting a linear model of expression during chondrogenic differentiation (R^2 = 0.8 and p value <0.05) in CPC^{Control}, but not in CPC$^{RAB5C-/-}$.

(B) qPCR analysis of *BMPR1B* (n = 5), *IL4R* (n = 5), *NOTCH3* (n = 5) and *SMAD7* (n = 5) expression in CPC^{Control} and CPC$^{RAB5C-/-}$ on days 0, 3 and 28, with graphs representing means ± SD. ANOVA followed by Tukey's post hoc test, *p < 0.05.

modulates pre-hypertrophic chondrogenesis independent from SOX9 is further corroborated by the findings of Chen et al. (2014), who reported that RUNX2 already plays an important role in earlier stages of development. The COL2a-Cre driven expression of a truncated RUNX2 protein resulted in distorted growth plate architecture, including decreased chondrocyte numbers in resting, proliferating, and pre-hypertrophic regions of mice. However, they did not observe differences in the SOX9 level between wild-type and mutant limbs, again indicating that RUNX2 modulates chondrogenesis independent of the SOX9 level. Nevertheless, neither Chen et al. (2014) nor we investigated whether the RUNX2 deletion alters the regulation of SOX9 activity by phosphorylation (Huang et al., 2000) or translocation (Malki et al., 2005) in addition to the actual level of the SOX9 protein.

RAB5C is a potential target that enhances chondrogenesis in CPCs

Previous studies have focused on altering the ECM synthesis of chondrocytes and CPCs through stimulation with growth factors (Janssen et al., 2019; Gelse et al., 2008; Wagner et al., 2019). However, the complexity of the underlying mechanisms often leads to ambiguous results, as the same ligand may trigger different responses (Grafe et al., 2018; Kozhemyakina et al., 2015). Here, we successfully avoided this issue by identifying RAB5C as potential interaction partner of SOX9. RAB proteins are attractive drug targets (Russell, 2007; Coxon et al., 2005). The deletion of RAB5C resulted in an increase in the expression of several chondrogenic markers, including the SOX trio. Increased expression of chondrogenic marker genes has produced promising results *in vivo* (Jeong et al., 2020; Im and Kim, 2011). Consistent with the findings from our previous study (Koelling et al., 2009), a reduction in RUNX2 expression in CPC$^{RAB5C-/-}$ correlated with an increased expression of chondrogenic markers. The loss of RAB5C did not impair ACAN and COL2 deposition, cell proliferation and the formation of cell clusters in 3D alginate beads *in vivo*. These cell clusters are also observed in OA tissue (Poole et al., 1991), and their formation has been proposed as the initial step of cartilage regeneration (Lotz et al., 2010).

In addition to the increased deposition of COL2, the amount of fibrotic COL1 was not affected by the loss of RAB5C. Thus, an upregulation of chondrogenic markers does not necessarily suppress the fibrotic traits of

CPCs, and therapies simply aiming to increase the chondrogenic potential of CPCs would not result in the complete absence of fibrocartilage in patients. Nevertheless, the deposition of more chondrogenic fibrocartilage with a higher amount of COL2 would postpone the total loss of joint function and thus improve the quality of life of patients.

The loss of RAB5C alters receptor expression in CPCs

The increased expression of several chondrogenic markers observed after the loss of RAB5C indicated an upstream repressor function of RAB5C. The further investigation of this interaction did not reveal a co-localization of SOX9 and RAB5C *in vitro*, although RAB5C was identified using the SOX9-His pulldown. The loss of RAB5C did not alter the localization of RUNX2, a known modulator of SOX9 function (Zhou et al., 2006). A limitation of our study is that the levels of SOX9 and RUNX2 activity, e.g., phosphorylation, were not measured. As no literature is available that indicates a physical interaction between RAB5C and one of the two proteins, we assume that the pro-chondrogenic effect results from altered signaling events. Although RAB5C has been linked to EGF signaling (Miaczynska et al., 2004) and another RAB protein, RAB23, indirectly regulates SOX9 through SHH signaling (Yang et al., 2008), our data suggested alterations in BMP, Notch, and IL signaling after loss of RAB5C in CPCs.

First, BMP receptors bind to multiple ligands involved in chondrogenesis (Grafe et al., 2018), and activate small mothers against decapentaplegic (SMADs) (Mummery, 2001). Interestingly, BMPR1B was described to exert overlapping functions with BMPR1A in mice, and decreased expression of the SOX trio was observed in Bmpr1aCKO; Bmpr1b$^{-/-}$ mice (Yoon et al., 2005). However, according to Kaps et al. (2004), BMPR1B is unlikely to play a role in chondrogenesis of mesenchymal progenitors. Future studies should include analyses of the levels of phosphorylated SMAD7 due to its co-localization to early endosomes (Rajagopal et al., 2007) and its inhibitory function in BMP signaling (Mummery, 2001).

As shown in a study by Green et al. (2015), transient Notch signaling is necessary for chondrogenesis, as Notch receptors are present in chondroprogenitors and their spatial expression changes during cartilage development. Consistent with this finding, Oldershaw et al. (2008) observed peak levels of NOTCH3 in hMSC2D monoculture, but decreased levels were observed in the subsequent 3D chondrogenic pellet culture. Thus, this pathway is important for the initiation of chondrogenesis and must be inhibited in the initial step. Whereas the 3D chondrogenic pellet culture mimics the process of endochondral condensation during embryonic development, the 3D alginate culture resembles chondrocytes in the adult joint and is characterized by few cell-cell contacts on which Notch signaling usually depends. Therefore, the downregulation of NOTCH3 in confluent cells exerts a pro-chondrogenic effect that is usually not observed in 3D alginate culture and the loss of RAB5C in 3D alginate culture could mimic this effect through the downregulation of NOTCH3. However, soluble ligands of Notch receptors have also recently been identified (D'souza et al., 2008).

IL4-mediated activation of JAK/STAT signaling has been investigated in chondrocytes from healthy and OA cartilage. The authors proposed that a crosstalk with integrins and other cytokine signaling pathways rather than the level of IL4R expression that play important roles in mechanotransduction and cartilage degradation (Millward-Sadler et al., 2006). Assirelli et al. (2014) did not detect differences in IL4R expression in healthy and OA cartilage specimens and highlighted the difference in the expression level of the ligand IL4.

Additional studies on the protein levels of the candidate genes are required to elucidate the mechanism underlying the effect of RAB5C on the aforementioned signaling pathways.

Taken together, our study highlights the pro-chondrogenic effect of the osteogenic regulator RUNX2, whose deletion negatively regulates ECM synthesis in CPCs. Furthermore, RAB5C was newly identified as a protein that enhances chondrogenesis. Its deletion enhances the chondrogenic potential of CPCs *in vitro*, an effect that is likely mediated by altered BMP, Notch, and IL signaling. More research on the *in vivo* phenotype and the underlying signaling pathways is necessary to further endorse RAB5C as a potential target for future OA therapies.

Limitations of the study

We acknowledge several limitations to the study presented here. In this work, we identified potential interaction partners of SOX9 by a pulldown experiment. Using Δbait; CPC^{Control} instead of Δbait; CPC^{siRUNX2} as

control, we cannot exclude that the siRNA transfection affected the background binding. Furthermore, as we did not elucidate a direct physical interaction of the endosomal marker RAB5C with SOX9 or RUNX2, it is possible that the pro-chondrogenic effect observed after the loss of RAB5C is related to an endosomal cargo protein. Finally, we previously demonstrated that sex-specific differences influence the regulation of gene expression in CPCs. Therefore, we cannot exclude that the results represented here for the female CPC241hT cell line could deviate in cell lines originating from male patients. We look forward to address this in our future studies.

Resource availability

Lead contact

Further information and requests for resources and reagents should be directed to and will be fulfilled by the Lead Contact, Nicolai Miosge (nmiosge@gwdg.de).

Materials availability

All cell lines and plasmids generated in this study will be made available on request.

Data and code availability

The RNA-Seq datasets are available at NCBI Gene Expression Omnibus (GEO), GEO accession: GSE158463. The mass spectrometry proteomics data have been deposited into the ProteomeXchange Consortium via the PRIDE partner repository (Perez-Riverol et al., 2015), PXD accession: PXD021785.

METHODS

All methods can be found in the accompanying transparent methods supplemental file.

SUPPLEMENTAL INFORMATION

Supplemental information can be found online at https://doi.org/10.1016/j.isci.2021.102464.

ACKNOWLEDGMENTS

We would like to thank the staff of the Transcriptome and Genome Analysis Laboratory (TAL) Göttingen, particularly Dr. Gabriela Salinas-Riester and Orr Shomroni, for performing the RNA-Seq analysis and the UMG Core Facility Proteomics, particularly Lisa Neuenroth, for providing expert technical advice. The authors disclosed the receipt of the following financial support for the research, authorship, and/or publication of this article: The Deutsche Forschungsgemeinschaft (Mi-573/10-2) and partial support from the Göttingen Graduate School for Neurosciences, Biophysics, and Molecular Biosciences (GSC 226/4).

AUTHOR CONTRIBUTIONS

JNJ contributed to the study conception, study design, analyses and interpretation of data, figure preparation, manuscript preparation, and statistical analyses. NM contributed to the study conception, study design, interpretation of data, and manuscript preparation. GC, CB, EH, DK, FL, and RN assisted with the experiments. CL designed and assisted with the experiments. VI performed computational and statistical analyses. VR contributed to the study conception, experimental design and interpretation of data.

DECLARATION OF INTERESTS

The authors have no potential conflicts of interest to declare with respect to the research, authorship, and/or publication of this article.

Inclusion and Diversity statement: We worked to ensure gender balance and ethnic or other types of diversity in the recruitment of human subjects. One or more of the authors of this paper self-identifies as a member of the LGBTQ+ community.

Received: November 17, 2020
Revised: February 24, 2021
Accepted: April 21, 2021
Published: May 21, 2021

REFERENCES

Albus, E., Sinningen, K., Winzer, M., Thiele, S., Baschant, U., Hannemann, A., Fantana, J., Tausche, A.K., Wallaschofski, H., Nauck, M., et al. (2016). Milk fat globule-epidermal growth factor 8 (MFG-E8) is a novel anti-inflammatory factor in rheumatoid arthritis in mice and humans. J. Bone Miner. Res. *31*, 596–605.

Assirelli, E., Pulsatelli, L., Dolzani, P., Platano, D., Olivotto, E., Filardo, G., Trisolino, G., Facchini, A., Borzì, R.M., and Meliconi, R. (2014). Human osteoarthritic cartilage shows reduced in vivo expression of IL-4, a chondroprotective cytokine that differentially modulates IL-1β-stimulated production of chemokines and matrix-degrading enzymes in vitro. PLoS One *9*, e96925.

Bi, W., Deng, J.M., Zhang, Z., Behringer, R.R., and De Crombrugghe, B. (1999). Sox9 is required for cartilage formation. Nat. Genet. *22*, 85–89.

Bi, W., Huang, W., Whitworth, D.J., Deng, J.M., Zhang, Z., Behringer, R.R., and De Crombrugghe, B. (2001). Haploinsufficiency of Sox9 results in defective cartilage primordia and premature skeletal mineralization. Proc. Natl. Acad. Sci.U S A *98*, 6698–6703.

Brittberg, M., Lindahl, A., Nilsson, A., Ohlsson, C., Isaksson, O., and Peterson, L. (1994). Treatment of deep cartilage defects in the knee with autologous chondrocyte transplantation. N. Engl. J. Med. *331*, 889–895.

Buckwalter, J.A., and Mankin, H.J. (1998). Articular cartilage: degeneration and osteoarthritis, repair, regeneration, and transplantation. Instr. Course Lect. *47*, 487–504.

Chen, H., Ghori-Javed, F.Y., Rashid, H., Adhami, M.D., Serra, R., Gutierrez, S.E., and Javed, A. (2014). Runx2 regulates endochondral ossification through control of chondrocyte proliferation and differentiation. J. Bone Miner. Res. *29*, 2653–2665.

Cheng, A., and Genever, P.G. (2010). Sox9 determines RUNX2 transactivity by directing intracellular degradation. J Bone Miner Res *12*, 2680–2689.

Coxon, F.P., Ebetino, F.H., Mules, E.H., Seabra, M.C., Mckenna, C.E., and Rogers, M.J. (2005). Phosphonocarboxylate inhibitors of Rab geranylgeranyl transferase disrupt the prenylation and membrane localization of Rab proteins in osteoclasts in vitro and in vivo. Bone *37*, 349–358.

D'souza, B., Miyamoto, A., and Weinmaster, G. (2008). The many facets of Notch ligands. Oncogene *27*, 5148–5167.

Dai, H., Chen, R., Gui, C., Tao, T., Ge, Y., Zhao, X., Qin, R., Yao, W., Gu, S., Jiang, Y., and Gui, J. (2020). Eliminating senescent chondrogenic progenitor cells enhances chondrogenesis under intermittent hydrostatic pressure for the treatment of OA. Stem Cell Res. Ther. *11*, 199.

De Crombrugghe, B., Lefebvre, V., and Nakashima, K. (2001). Regulatory mechanisms in the pathways of cartilage and bone formation. Curr.Opin.Cell Biol. *13*, 721–727.

Embree, M.C., Chen, M., Pylawka, S., Kong, D., Iwaoka, G.M., Kalajzic, I., Yao, H., Shi, C., Sun, D., Sheu, T.J., et al. (2016). Exploiting endogenous fibrocartilage stem cells to regenerate cartilage and repair joint injury. Nat. Commun. *7*, 13073.

Eyre, D.R. (1991). The collagens of articular cartilage. Semin. Arthritis Rheum. *21*, 2–11.

Felson, D.T. (2006). Osteoarthritis of the knee. N. Engl. J. Med. *354*, 841–848.

Gelse, K., Mühle, C., Knaup, K., Swoboda, B., Wiesener, M., Hennig, F., Olk, A., and Schneider, H. (2008). Chondrogenic differentiation of growth factor-stimulated precursor cells in cartilage repair tissue is associated with increased HIF-1alpha activity. Osteoarthritis Cartilage *16*, 1457–1465.

Goldring, M.B., and Goldring, S.R. (2007). Osteoarthritis. J.Cell. Physiol. *213*, 626–634.

Grafe, I., Alexander, S., Peterson, J.R., Snider, T.N., Levi, B., Lee, B., and Mishina, Y. (2018). TGF-βfamily signaling in mesenchymal differentiation. Cold Spring Harb. Perspect. Biol. *10*, a022202.

Green, J.D., Tollemar, V., Dougherty, M., Yan, Z., Yin, L., Ye, J., Collier, Z., Mohammed, M.K., Haydon, R.C., Luu, H.H., et al. (2015). Multifaceted signaling regulators of chondrogenesis: implications in cartilage regeneration and tissue engineering. Genes Dis. *2*, 307–327.

Hanley, K.P., Oakley, F., Sugden, S., Wilson, D.I., Mann, D.A., and Hanley, N.A. (2008). Ectopic SOX9 mediates extracellular matrix deposition characteristic of organ fibrosis. J. Biol. Chem. *283*, 14063–14071.

Heinegard, D., and Saxne, T. (2011). The role of the cartilage matrix in osteoarthritis. Nat. Rev. Rheumatol. *7*, 50–56.

Horton, W.E., Jr., Bennion, P., and Yang, L. (2006). Cellular, molecular, and matrix changes in cartilage during aging and osteoarthritis. J. Musculoskelet. Neuronal Interact. *6*, 379–381.

Huang, W., Zhou, X., Lefebvre, V., and De Crombrugghe, B. (2000). Phosphorylation of SOX9 by cyclic AMP-dependent protein kinase A enhances SOX9's ability to transactivate a Col2a1 chondrocyte-specific enhancer. Mol.Cell. Biol. *20*, 4149–4158.

Huang, Y.H., Jankowski, A., Cheah, K.S., Prabhakar, S., and Jauch, R. (2015). SOXE transcription factors form selective dimers on non-compact DNA motifs through multifaceted interactions between dimerization and high-mobility group domains. Sci. Rep. *5*, 10398.

Im, G.I., and Kim, H.J. (2011). Electroporation-mediated gene transfer of SOX trio to enhance chondrogenesis in adipose stem cells. Osteoarthritis Cartilage *19*, 449–457.

Inada, M., Yasui, T., Nomura, S., Miyake, S., Deguchi, K., Himeno, M., Sato, M., Yamagiwa, H., Kimura, T., Yasui, N., et al. (1999). Maturational disturbance of chondrocytes in Cbfa1-deficient mice. Dev. Dyn. *214*, 279–290.

Izzi, V., Lakkala, J., Devarajan, R., Kääriäinen, A., Koivunen, J., Heljasvaara, R., and Pihlajaniemi, T. (2019). Pan-Cancer analysis of the expression and regulation of matrisome genes across 32 tumor types. Matrix Biol. Plus *1*, 1–13.

Janssen, J.N., Batschkus, S., Schimmel, S., Bode, C., Schminke, B., and Miosge, N. (2019). The influence of TGF-β3, EGF, and BGN on SOX9 and RUNX2 expression in human chondrogenic progenitor cells. J. Histochem.Cytochem. *67*, 117–127.

Jenei-Lanzl, Z., Grässel, S., Pongratz, G., Kees, F., Miosge, N., Angele, P., and Straub, R.H. (2014). Norepinephrine inhibition of mesenchymal stem cell and chondrogenic progenitor cell chondrogenesis and acceleration of chondrogenic hypertrophy. Arthritis Rheumatol. *66*, 2472–2481.

Jeong, S.Y., Kang, M.L., Park, J.W., and Im, G.I. (2020). Dual functional nanoparticles containing SOX duo and ANGPT4 shRNA for osteoarthritis treatment. J. Biomed.Mater. Res. B Appl. Biomater. *108*, 234–242.

Jo, A., Denduluri, S., Zhang, B., Wang, Z., Yin, L., Yan, Z., Kang, R., Shi, L.L., Mok, J., Lee, M.J., and Haydon, R.C. (2014). The versatile functions of Sox9 in development, stem cells, and human diseases. Genes Dis. *1*, 149–161.

Joos, H., Wildner, A., Hogrefe, C., Reichel, H., and Brenner, R.E. (2013). Interleukin-1 beta and tumor necrosis factor alpha inhibit migration activity of chondrogenic progenitor cells from non-fibrillated osteoarthritic cartilage. Arthritis Res. Ther. *15*, R119.

Kaps, C., Hoffmann, A., Zilberman, Y., Pelled, G., Häupl, T., Sittinger, M., Burmester, G., Gazit, D., and Gross, G. (2004). Distinct roles of BMP receptors Type IA and IB in osteo-/chondrogenic differentiation in mesenchymal progenitors (C3H10T1/2). Biofactors *20*, 71–84.

Kim, I.S., Otto, F., Zabel, B., and Mundlos, S. (1999). Regulation of chondrocyte differentiation by Cbfa1. Mech. Dev. *80*, 159–170.

Koelling, S., Kruegel, J., Irmer, M., Path, J.R., Sadowski, B., Miro, X., and Miosge, N. (2009). Migratory chondrogenic progenitor cells from repair tissue during the later stages of human osteoarthritis. Cell Stem Cell *4*, 324–335.

Kozhemyakina, E., Lassar, A.B., and Zelzer, E. (2015). A pathway to bone: signaling molecules and transcription factors involved in chondrocyte development and maturation. Development *142*, 817–831.

Kumar, D., and Lassar, A.B. (2009). The transcriptional activity of Sox9 in chondrocytes is regulated by RhoA signaling and actin polymerization. Mol.Cell. Biol *29*, 4262–4273.

Lefebvre, V., Huang, W., Harley, V.R., Goodfellow, P.N., and De Crombrugghe, B. (1997). SOX9 is a potent activator of the chondrocyte-specific enhancer of the pro alpha1(II) collagen gene. Mol.Cell. Biol *17*, 2336–2346.

Lohmander, L.S., and Roos, E.M. (2007). Clinical update: treating osteoarthritis. Lancet *370*, 2082–2084.

Lotz, M.K., Otsuki, S., Grogan, S.P., Sah, R., Terkeltaub, R., and D'lima, D. (2010). Cartilage cell clusters. Arthritis Rheum. *62*, 2206–2218.

Malki, S., Nef, S., Notarnicola, C., Thevenet, L., Gasca, S., Méjean, C., Berta, P., Poulat, F., and Boizet-Bonhoure, B. (2005). Prostaglandin D2 induces nuclear import of the sex-determining factor SOX9 via its cAMP-PKA phosphorylation. EMBO J. *24*, 1798–1809.

Matta, C., Boocock, D.J., Fellows, C.R., Miosge, N., Dixon, J.E., Liddell, S., Smith, J., and Mobasheri, A. (2019). Molecular phenotyping of the surfaceome of migratory chondroprogenitors and mesenchymal stem cells using biotinylation, glycocapture and quantitative LC-MS/MS proteomic analysis. Sci. Rep. *9*, 9018.

Mendler, M., Eich-Bender, S.G., Vaughan, L., Winterhalter, K.H., and Bruckner, P. (1989). Cartilage contains mixed fibrils of collagen types II, IX, and XI. J.Cell Biol. *108*, 191–197.

Miaczynska, M., Christoforidis, S., Giner, A., Shevchenko, A., Uttenweiler-Joseph, S., Habermann, B., Wilm, M., Parton, R.G., and Zerial, M. (2004). APPL proteins link Rab5 to nuclear signal transduction via an endosomal compartment. Cell *116*, 445–456.

Millward-Sadler, S.J., Khan, N.S., Bracher, M.G., Wright, M.O., and Salter, D.M. (2006). Roles for the interleukin-4 receptor and associated JAK/STAT proteins in human articular chondrocyte mechanotransduction. Osteoarthritis Cartilage *14*, 991–1001.

Miosge, N., Hartmann, M., Maelicke, C., and Herken, R. (2004). Expression of collagen type I and type II in consecutive stages of human osteoarthritis. Histochem.Cell Biol. *122*, 229–236.

Miosge, N., Waletzko, K., Bode, C., Quondamatteo, F., Schultz, W., and Herken, R. (1998). Light and electron microscopic in-situ hybridization of collagen type I and type II mRNA in the fibrocartilaginous tissue of late-stage osteoarthritis. Osteoarthritis Cartilage *6*, 278–285.

Mummery, C.L. (2001). Transforming growth factor β and mouse development. Microsc. Res. Tech. *52*, 374–386.

Nefla, M., Sudre, L., Denat, G., Priam, S., Andre-Leroux, G., Berenbaum, F., and Jacques, C. (2015). The pro-inflammatory cytokine 14-3-3ε is a ligand of CD13 in cartilage. J.Cell Sci. *128*, 3250–3262.

Oldberg, Å., Antonsson, P., Hedbom, E., and Heinegard, D. (1990). Structure and function of extracellular matrix proteoglycans. Biochem. Soc. Trans. *18*, 789–792.

Oldershaw, R.A., Tew, S.R., Russell, A.M., Meade, K., Hawkins, R., Mckay, T.R., Brennan, K.R., and Hardingham, T.E. (2008). Notch signaling through Jagged-1 is necessary to initiate chondrogenesis in human bone marrow stromal cells but must be switched off to complete chondrogenesis. Stem Cells *26*, 666–674.

Otto, F., Thornell, A.P., Crompton, T., Denzel, A., Gilmour, K.C., Rosewell, I.R., Stamp, G.W., Beddington, R.S., Mundlos, S., Olsen, B.R., et al. (1997). Cbfa1, a candidate gene for cleidocranial dysplasia syndrome, is essential for osteoblast differentiation and bone development. Cell *89*, 765–771.

Perez-Riverol, Y., Alpi, E., Wang, R., Hermjacob, H., and Vizcaino, J.A. (2015). Making proteomics data accessible and re-usable: current state of proteomics databases and repositoris. Proteomics *15*, 930–950.

Poole, C.A. (1997). Articular cartilage chondrons: form, function and failure. J. Anat. *191* (Pt 1), 1–13.

Poole, C.A., Matsuoka, A., and Schofield, J.R. (1991). Chondrons from articular cartilage. III. Morphologic changes in the cellular microenvironment of chondrons isolated from osteoarthritic cartilage. Arthritis Rheum. *34*, 22–35.

Pratap, J., Lian, J.B., and Stein, G.S. (2011). Metastatic bone disease: role of transcription factors and future targets. Bone *48*, 30–36.

Pritchett, J., Athwal, V., Roberts, N., Hanley, N.A., and Hanley, K.P. (2011). Understanding the role of SOX9 in acquired diseases: lessons from development. Trends Mol. Med. *17*, 166–174.

Rajagopal, R., Ishii, S., and Beebe, D.C. (2007). Intracellular mediators of transforming growth factor beta superfamily signaling localize to endosomes in chicken embryo and mouse lenses in vivo. BMC Cell Biol. *8*, 25.

Reginster, J.Y. (2002). The prevalence and burden of arthritis. Rheumatology (Oxford) *41* (Supp 1), 3–6.

Russell, R.G. (2007). Bisphosphonates: mode of action and pharmacology. Pediatrics *119* (*Suppl 2*), S150–S162.

Sandell, L.J., and Aigner, T. (2001). Articular cartilage and changes in arthritis. An introduction: cell biology of osteoarthritis. Arthritis Res. *3*, 107–113.

Schminke, B., and Miosge, N. (2014). Cartilage repair in vivo: the role of migratory progenitor cells. Curr.Rheumatol.Rep. *16*, 461.

Seol, D., Mccabe, D.J., Choe, H., Zheng, H., Yu, Y., Jang, K., Walter, M.W., Lehman, A.D., Ding, L., Buckwalter, J.A., and Martin, J.A. (2012). Chondrogenic progenitor cells respond to cartilage injury. Arthritis Rheum. *64*, 3626–3637.

Setton, L.A., Elliott, D.M., and Mow, V.C. (1999). Altered mechanics of cartilage with osteoarthritis: human osteoarthritis and an experimental model of joint degeneration. Osteoarthritis Cartilage *7*, 2–14.

Valenti, M.T., Serafini, P., Innamorati, G., Gili, A., Cheri, S., Bassi, C., and Dalle Carbonare, L. (2016). Runx2 expression: a mesenchymal stem marker for cancer. Oncol.Lett. *12*, 4167–4172.

Wagner, G., Lehmann, C., Bode, C., Miosge, N., and Schubert, A. (2019). High mobility group box 1 protein in osteoarthritic knee tissue and chondrogenic progenitor cells: an ex vivo and in vitro study. Cartilage, 1947603519835897.

Wang, K., Li, J., Li, Z., Wang, B., Qin, Y., Zhang, N., Zhang, H., Su, X., Wang, Y., and Zhu, H. (2019). Chondrogenic progenitor cells exhibit superiority over mesenchymal stem cells and chondrocytes in platelet-rich plasma scaffold-based cartilage regeneration. Am. J. Sports Med. *47*, 2200–2215.

Wang, R., Jiang, W., Zhang, L., Xie, S., Zhang, S., Yuan, S., Jin, Y., and Zhou, G. (2020). Intra-articular delivery of extracellular vesicles secreted by chondrogenic progenitor cells from MRL/MpJ superhealer mice enhances articular cartilage repair in a mouse injury model. Stem Cell Res. Ther. *11*, 93.

WHO (2013). Priority Diseases and Reason for Inclusion. http://www.who.int/medicines/areas/priority_medicines/Ch6_12Osteo.pdf.

Yang, L., Clinton, J.M., Blackburn, M.L., Zhang, Q., Zou, J., Zielinska-Kwiatkowska, A., Tang, B.L., and Chansky, H.A. (2008). Rab23 regulates differentiation of ATDC5 chondroprogenitor cells. J. Biol. Chem. *283*, 10649–10657.

Yoon, B.S., Ovchinnikov, D.A., Yoshii, I., Mishina, Y., Behringer, R.R., and Lyons, K.M. (2005). Bmpr1a and Bmpr1b have overlapping functions and are essential for chondrogenesis in vivo. Proc. Natl. Acad. Sci.U S A *102*, 5062–5067.

Zhou, G., Zheng, Q., Engin, F., Munivez, E., Chen, Y., Sebald, E., Krakow, D., and Lee, B. (2006). Dominance of SOX9 function over RUNX2 during skeletogenesis. Proc. Natl. Acad. Sci. U S A *103*, 19004–19009.

iScience, Volume *24*

Supplemental information

Enhancing the chondrogenic potential of chondrogenic progenitor cells by deleting RAB5C

Jerome Nicolas Janssen, Valerio Izzi, Elvira Henze, Gökhan Cingöz, Florian Lowen, David Küttner, Ruth Neumann, Christof Lenz, Vicki Rosen, and Nicolai Miosge

Transparent Methods

Cell isolation and culture

4 CPC lines (CPC241, CPC674, CPC677, and CPC678) from patients (2 males and 2 females, age 61-82 years, height 156-185 cm, weight 60-110 kg) were established by collecting 5 to 10 mm^3 tissue samples from histopathologically confirmed late-stage OA tissue (Pritzker et al., 2006). The tissue samples were added to a cell culture dish, washed and cultivated under standard conditions at 37°C with 5% CO_2 in DMEM + GlutaMax™ supplemented with 10% FCS and 50 µg/mL gentamycin. After 10 days, outgrown cells were harvested, transferred to a 75 cm^2 flask (Janssen et al., 2019, Koelling et al., 2009). A lentivirus expressing hTERT was produced as described in a previous study (Docheva et al., 2010). The pLenti6/v5-hTERT plasmid was cotransfected with pLP1, pLP2, and pLP/VSVG helper plasmids (ViraPower lentiviral expression system, Invitrogen) in 293FT cells, and the supernatant was collected after 48 h. CPCs were infected with the hTERT lentivirus (moi of 5×10^4) and selected with 10 µg/mL blasticidin for 1 week.

Chondrogenic differentiation

First, 7×10^5 cells were embedded in sterile 1.2% FMC Biopolymer alginate (Häuselmann et al., 1994, Koelling et al., 2009) and cultured with standard DMEM supplemented with 3.9 µM/100 mL dexamethasone, 10 mg/mL Na-pyruvate, 4 mg/100 mL L-proline, 5 mg/100 mL ascorbate and 5 µL/mL ITS for up to 28 days. Cells were retrieved from beads using HEPES-EDTA.

Data-independent acquisition mass spectrometry

CPCs from patients were differentiated towards the chondrogenic lineage. On day 27, the medium was changed to FCS-free chondrogenic medium. SDS-PAGE, in-gel trypsin digestion, extraction and MS were performed using the methods described in a previous study (Batschkus et al., 2017). For the generation of a peptide library, equal amount aliquots from each sample were pooled to a total amount of 150 µg, dried in a vacuum concentrator and resuspended in 0.1% TFA. The pool was then separated into 14 fractions using reverse-phase chromatography (1.0 mm ID x 150 mm, Hypersil Gold C18 aq, 5 µm, Thermo Fisher Scientific) with 5-40% acetonitrile/0.01 M ammonium hydroxide (pH 8.0) at a rate of 200 µL min^{-1} and a staggered pooling scheme (1+15+29).

For mass spectrometry, peptide samples were reconstituted in 2% acetonitrile/0.1% formic acid (v:v) and spiked with a synthetic peptide standard used for retention time alignment (iRT Standard). Samples were analyzed using a nanoflow chromatography system coupled to a hybrid triple quadrupole-TOF mass spectrometer using the method described in a previous study (Erdmann et al., 2019).

Proteins were identified using ProteinPilot Software v5.0 build 4769 (AB Sciex) and "thorough" settings. The combined qualitative analyses were searched against the UniProtKB human reference proteome (revision 04-2018, 93,609 entries) augmented with a set of 52 known common laboratory contaminants to identify proteins at a False Discovery Rate (FDR) of 1%.

Spectral library generation and peak extraction were achieved with PeakView Software v2.1 build 11041 (AB Sciex) using the SWATH quantitation microApp v2.0 build 2003. Following the retention time correction using the iRT standard, peak areas were extracted using information from the MS/MS library at an FDR of 1% (Lambert et al., 2013). The resulting peak areas were then summed to peptide and finally protein area values per injection, which were used for further statistical analysis. Cell lines were grouped together (CPC677 and CPC241hT, CPC674 and CPC674hT, and CPC678 and CPC678hT), and proteins were compared using the Mann-Whitney U test with the FDR correction. Significant proteins were selected by thresholding at a p value < 0.05, divided into up-and down-regulated by fold change (primary or immortalized). Proteins up- or down-regulated were enriched for GO biological processes (GO:BP) using the ClusterProfiler package and a FDR-corrected enrichment thresholding at a p value < 0.05.

Generation of $CPC^{siRUNX2}$, $CPC^{RUNX2-/-}$ and $CPC^{RAB5C-/-}$

For the knockdown, 1×10^6 CPC241hT cells were transfected with 2 µg of piLenti-siRNA-GFP-RUNX2-1472 (TGGATGAATCTGTTTGGCGACCATATTGA) (BioCat), or for the knockout, cells were transfected with 2 µg each of pSp-Cas9(BB)-2A-GFP (Addgene) vector pairs (inserts: RAB5C: 5' GAAGAGAGAAGGAGCGTCCAT, 5' GGGTTAAGCGGCCTGAAATC; RUNX2: 5' GCCGGCCACTTCGCTAACTTG, 5' GAGGTCTTGGAGGACGTCCG) in 100 µL of the Human Nucleofector Solution (Amaxa) using nucleofector program C17 (Amaxa). Immediately afterwards, the cells were cultured under standard conditions. Following piLenti-siRNA-GFP-RUNX2-1472 transfection, dead cells were decanted after 16 h (Koelling et al., 2009). pSp-Cas9(BB)-2A-GFP transfected cells were sorted by FACS to separate one cell per well, gDNA was isolated (Kappa mouse genotyping kit KK7103) and loci were sequenced using the following primers: RAB5C: 5'

CCCTAGCTGCTGGTCTGTTC, 5' TCAAGTGATCCTCCCACTCC; and RUNX2: 5' TCAGACAGAGGTGGGGGTAG, 5' AGACCTGAGGAGAGGCGTTT.

Real-time polymerase chain reaction (RT-PCR)

RT-qPCR was performed using 5 µL of SsoAdvanced Universal SYBR Green Supermix (Bio-Rad), 20 pmol of each primer and 1 ng of cDNA in a total volume of 10 µL (Koelling et al., 2009). Analysis was performed using the ΔΔCT method (Livak and Schmittgen, 2001). The primers are listed in Table S5. At least 3 replicates were analyzed using Student's t-test or ANOVA followed by Tukey's post hoc test, * $p < 0.05$.

Immunoblotting

Protein levels were determined using SDS-PAGE and Western blotting with PVDF membranes. TBS-T was used for washing and 5% milk powder in TBS-T was used for blocking (Janssen et al., 2019, Koelling et al., 2009). Primary antibodies were diluted as follows and incubated with the membrane overnight: RUNX2: 1:2000, polyclonal rabbit ab23981 (Abcam); SOX9: 1:2000, monoclonal mouse H00006662-M02 (Abnova); COL1: 1:500, polyclonal rabbit R1038 (Acris); COL2A1: 1:300, monoclonal mouse sc-51801 (Santa Cruz); RAB5C: 1:500, monoclonal mouse sc-365667 (Santa Cruz); Anti-6X His tag®: 1:2000, monoclonal mouse ab18184 (Abcam). Secondary antibodies were diluted as follows and incubated with the membrane for 1 h: polyclonal goat anti-mouse A 9917, 1:40000 (Sigma-Aldrich) and polyclonal goat anti-rabbit, A 0545, 1:100000 (Sigma-Aldrich). WesternBright™ Sirius (K-12043-D20, Biozym) and WesternBright™ ECL (K-12045-D20, Biozym) were used for detection with a C-DiGit Blot Scanner. Protein levels were evaluated with Image Studio Digits v5.2 and normalized to the levels of α-tubulin (monoclonal mouse, T6199, 1:10000, Sigma-Aldrich) or GAPDH (monoclonal mouse ab9848, 1:5000, Abcam) (Gassmann et al., 2009). At least 3 replicates were analyzed using Student's t-test, * $p < 0.05$.

Pulldown and mass spectrometry analyses

HEK293T cells were transfected with pPM-hSOX9-His (PV132789, ABM) using PolyFect®. After 48h, cells were lysed and the released His-tagged protein was purified and incubated with HisPur™ Ni-NTA Magnetic beads in equilibrium buffer. Subsequently, the beads were washed and incubated with the lysate of $CPC^{siRUNX2}$ (Koelling et al., 2009) overnight at 4°C while rotating. Finally, the beads were washed and the protein complexes were eluted and

precipitated with ethanol. SDS-PAGE, in-gel trypsin digestion and extraction and MS were performed according to Batschkus et al. (2017) with slight alterations. Each lane was cut into 11 equidistant slices. Peptides were separated using a 37 min linear gradient (5-35%) and analyzed using a Top 10 data-dependent acquisition method. Three biological and two technical replicates were combined. Peak lists were extracted from the raw data with Raw2MSM v1.10 and analyzed using Mascot v2.4.1 by searching against the SwissProt database v2014_08 and validated with Scaffold v4.3.4. Spectral counting was used to determine relative protein abundances between samples (Lundgren et al., 2010). Spectral counts were normalized between the different samples using the DESeq method (Anders et al., 2013, Anders and Huber, 2010). Interacting proteins were identified using a two-stage Poisson model that was specifically adapted for spectral count data and included a biological and variance filter (Fischer et al., 2014). Differential binding between treatment and control groups was quantified by determining the log fold change using a FDR of 5%.

Ex vivo migration

For this experiment, 1 × 10^6 cells were transfected with 4 µg of pmaxGFP™ (Lonza) as described above. Osteoarthritic cartilage without signs of rheumatoid involvement were obtained from the knee joints of adult patients (1 male and 3 females, age 62-79 years, height 156-176 cm, weight 55-92 kg) suffering from late-stage OA after total knee replacement. The patients met the American College of Rheumatology classification criteria (Altman et al., 1986) and provided written informed consent, consistent with relevant ethical regulations (25/12/10). The histopathological classification of OA cartilage confirmed the presence of late-stage OA (Pritzker et al., 2006).

Animals

In vivo experiments using mice were performed in accordance with the Guide for the Care and Use of Laboratory Animals and were approved by the Harvard Medical Area Institutional Animal Care and Use Committee. Mice were maintained in a virus-and parasite-free barrier facility, housed on a 12-hour light/dark cycle and fed a standard diet with food and water available ad libitum. Female homozygous Foxn1nu mice were ordered from Jackson Lab (strain 002019 –NJ/J) and housed under sterile conditions. Cells used for implantation were embedded in 1.2% PRONOVA SLG100 alginate and 4 beads were transplanted into the back of 9 weeks old nude mice (7 mice for $CPC^{Control}$, 4 mice for $CPC^{RAB5C-/-}$, and 3 mice for

empty alginate beads). Mice were sacrificed after 28 days, the beads were retrieved and fixed for histology.

Immunohistochemistry and immunocytochemistry

IHC and ICC were performed as previously described (Schminke et al., 2016, Janssen et al., 2019). For IHC, tissue samples were fixed at 55 °C for 2 h. Primary antibodies were applied at the following dilutions for IHC: ACAN: 1:100, monoclonal mouse AHP0012 (Thermo Fisher); COL1: 1:50, polyclonal rabbit R1038 (Acris); COL2: 1:50, polyclonal rabbit NB100-91715 (Novus Biologicals); and KI-67: 1:50, monoclonal mouse M7240 (DakoCytomation). For detection, a HiDef Detection™ AlkPhos Polymer System (962D, Cell Marque) with PermaRed/AP-Auto (K049-Auto, Cell Marque) was applied. The following primary antibodies were applied for ICC: RAB5C: 1:50, monoclonal mouse sc-365667 (Santa Cruz); RUNX2: 1:20 polyclonal rabbit sc-10758 (Santa Cruz); and SOX9: 1:50, polyclonal rabbit sc-20095 (Santa Cruz). Alexa Fluor 555-conjugated polyclonal donkey anti-rabbit (ab150074, 1:500, Abcam) and DyLight 488-conjugated polyclonal goat anti-mouse (072-03-18-06, 1:500, KPL) secondary antibodies and a 1:1000 dilution of DAPI were applied for ICC.

RNA-Seq

Gene expression in $CPC^{Control}$ and $CPC^{RAB5C-/-}$ was measured on days 0, 3 and 28. Total RNA was isolated with an RNeasy kit (Qiagen). RNA-Seq libraries were prepared using TruSeq kits (Illumina). Samples were assessed for sequencing quality using FastQC v0.11.5 (Andrews, 2010). All experiments were performed in triplicate, and three biological replicates were sequenced per condition. SortMeRNA v2.1 (Kopylova et al., 2012) was used to determine the proportion of rRNAs in the samples. Human RNA-Seq data were aligned to the human genome assembly hg38 applying STAR v2.5.2a (Dobin et al., 2013) with the default options. The number of reads in each gene in the human genome v89 was quantified for every sample using FeatureCounts v1.5.0-p1 (Liao et al., 2014). All analyses were performed using R v4.0.1. Normalized gene-level RNA-Seq count tables were first averaged for duplicated genes, then divided into groups by genetic (RAB5C status) and time (0, 3 or 28 days) factors and analyzed. Differential gene expression was evaluated using DESeq2 v1.18.1 (Love et al., 2014) in count mode and global dispersion descriptors. For linear gene expression modeling of time and group ordered data, linear regression equations were fitted for each gene in both groups. The goodness-of-fit (R^2) and p value for each gene were compared between groups, and, depending whether a stringent or less stringent model was

used, regressor lists were established at cut-off values of $R^2 = 0.8$ and $p < 0.05$. Gene expression was considered altered in $CPC^{RAB5C-/-}$ if the genes were present in the $CPC^{Control}$ list but absent in the $CPC^{RAB5C-/-}$ list. Genes were further selected and compared using the Mann-Whitney U test with the FDR correction. The cartilage morphogenesis signature was downloaded from the MSigDB and the relative enrichment values were inferred for each sample using the “singScore” package in R. Differential enrichment was evaluated using the Mann-Whitney U test with the FDR correction. For GSEA, the differential expression analysis was performed between each set of $CPC^{Control}$ and $CPC^{RAB5C-/-}$ samples using DESeq2. The web service WebGestalt v0.4.3 (Liao et al., 2019) was applied to identify enriched GO categories and KEGG pathway terms (adjusted $p < 0.05$).

Supplemental References

ALTMAN, R., ASCH, E., BLOCH, D., BOLE, G., BORENSTEIN, D., BRANDT, K., CHRISTY, W., COOKE, T. D., GREENWALD, R., HOCHBERG, M. & ET AL. 1986. Development of criteria for the classification and reporting of osteoarthritis. Classification of osteoarthritis of the knee. Diagnostic and Therapeutic Criteria Committee of the American Rheumatism Association. *Arthritis Rheum,* 29**,** 1039-49.

ANDERS, S. & HUBER, W. 2010. Differential expression analysis for sequence count data. *Genome Biol,* 11**,** R106.

ANDERS, S., MCCARTHY, D. J., CHEN, Y., OKONIEWSKI, M., SMYTH, G. K., HUBER, W. & ROBINSON, M. D. 2013. Count-based differential expression analysis of RNA sequencing data using R and Bioconductor. *Nat Protoc,* 8**,** 1765-86.

ANDREWS, S. 2010. *FastQC: a quality control tool for high throughput sequence data* [Online]. Available: http://www.bioinformatics.babraham.ac.uk/projects/fastqc.

BATSCHKUS, S., ATANASSOV, I., LENZ, C., MEYER-MARCOTTY, P., CINGÖZ, G., KIRSCHNECK, C., URLAUB, H. & MIOSGE, N. 2017. Mapping the secretome of human chondrogenic progenitor cells with mass spectrometry. *Ann Anat,* 212**,** 4-10.

DOBIN, A., DAVIS, C. A., SCHLESINGER, F., DRENKOW, J., ZALESKI, C., JHA, S., BATUT, P., CHAISSON, M. & GINGERAS, T. R. 2013. STAR: ultrafast universal RNA-seq aligner. *Bioinformatics,* 29**,** 15-21.

DOCHEVA, D., PADULA, D., POPOV, C., WEISHAUPT, P., PRÄGERT, M., MIOSGE, N., HICKEL, R., BÖCKER, W., CLAUSEN-SCHAUMANN, H. & SCHIEKER, M. 2010. Establishment of immortalized periodontal ligament progenitor cell line and its behavioural analysis on smooth and rough titanium surface. *Eur Cell Mater,* 19**,** 228-41.

ERDMANN, J., THÖMING, J. G., POHL, S., PICH, A., LENZ, C. & HÄUSSLER, S. 2019. The Core Proteome of Biofilm-Grown Clinical Pseudomonas aeruginosa Isolates. *Cells,* 8.

FISCHER, M., ZILKENAT, S., GERLACH, R. G., WAGNER, S. & RENARD, B. Y. 2014. Pre- and post-processing workflow for affinity purification mass spectrometry data. *J Proteome Res,* 13**,** 2239-49.

GASSMANN, M., GRENACHER, B., ROHDE, B. & VOGEL, J. 2009. Quantifying Western blots: pitfalls of densitometry. *Electrophoresis,* 30**,** 1845-55.

HÄUSELMANN, H. J., FERNANDES, R. J., MOK, S. S., SCHMID, T. M., BLOCK, J. A., AYDELOTTE, M. B., KUETTNER, K. E. & THONAR, E. J. 1994. Phenotypic stability of bovine articular chondrocytes after long-term culture in alginate beads. *J Cell Sci,* 107 (Pt 1)**,** 17-27.

JANSSEN, J. N., BATSCHKUS, S., SCHIMMEL, S., BODE, C., SCHMINKE, B. & MIOSGE, N. 2019. The Influence of TGF-β3, EGF, and BGN on SOX9 and RUNX2 Expression in Human Chondrogenic Progenitor Cells. *J Histochem Cytochem,* 67**,** 117-127.

KOELLING, S., KRUEGEL, J., IRMER, M., PATH, J. R., SADOWSKI, B., MIRO, X. & MIOSGE, N. 2009. Migratory chondrogenic progenitor cells from repair tissue during the later stages of human osteoarthritis. *Cell Stem Cell,* 4**,** 324-35.

KOPYLOVA, E., NOÉ, L. & TOUZET, H. 2012. SortMeRNA: fast and accurate filtering of ribosomal RNAs in metatranscriptomic data. *Bioinformatics,* 28**,** 3211-7.

LAMBERT, J. P., IVOSEV, G., COUZENS, A. L., LARSEN, B., TAIPALE, M., LIN, Z. Y., ZHONG, Q., LINDQUIST, S., VIDAL, M., AEBERSOLD, R., PAWSON, T., BONNER, R., TATE, S. & GINGRAS, A. C. 2013. Mapping differential interactomes by affinity purification coupled with data-independent mass spectrometry acquisition. *Nat Methods,* 10**,** 1239-45.

LIAO, Y., SMYTH, G. K. & SHI, W. 2014. featureCounts: an efficient general purpose program for assigning sequence reads to genomic features. *Bioinformatics,* 30**,** 923-30.

LIAO, Y., WANG, J., JAEHNIG, E. J., SHI, Z. & ZHANG, B. 2019. WebGestalt 2019: gene set analysis toolkit with revamped UIs and APIs. *Nucleic Acids Res,* 47**,** W199-w205.

LIVAK, K. J. & SCHMITTGEN, T. D. 2001. Analysis of relative gene expression data using real-time quantitative PCR and the 2(-Delta Delta C(T)) Method. *Methods,* 25**,** 402-8.

LOVE, M. I., HUBER, W. & ANDERS, S. 2014. Moderated estimation of fold change and dispersion for RNA-seq data with DESeq2. *Genome Biol,* 15**,** 550.
LUNDGREN, D. H., HWANG, S. I., WU, L. & HAN, D. K. 2010. Role of spectral counting in quantitative proteomics. *Expert Rev Proteomics,* 7**,** 39-53.
PRITZKER, K. P., GAY, S., JIMENEZ, S. A., OSTERGAARD, K., PELLETIER, J. P., REVELL, P. A., SALTER, D. & VAN DEN BERG, W. B. 2006. Osteoarthritis cartilage histopathology: grading and staging. *Osteoarthritis Cartilage,* 14**,** 13-29.
SCHMINKE, B., TRAUTMANN, S., MAI, B., MIOSGE, N. & BLASCHKE, S. 2016. Interleukin 17 inhibits progenitor cells in rheumatoid arthritis cartilage. *Eur J Immunol,* 46**,** 440-5.

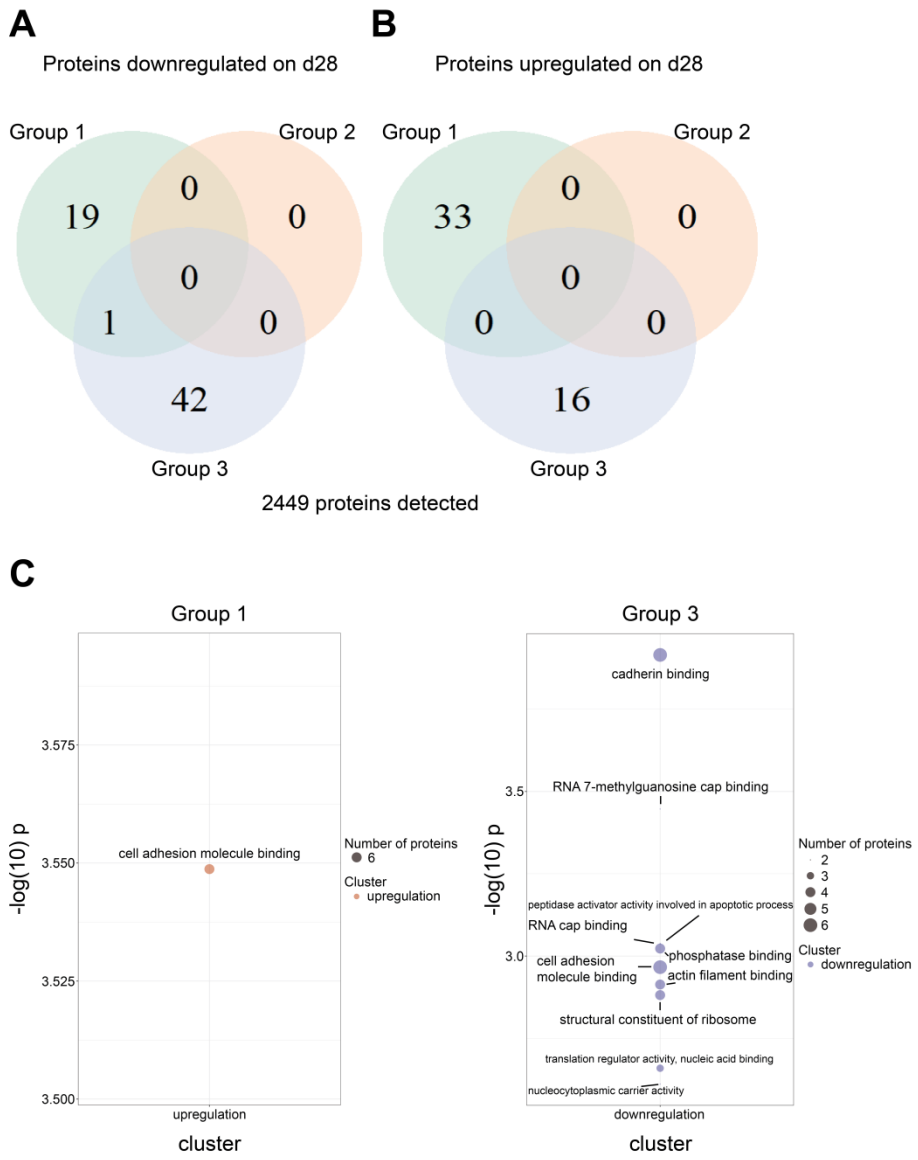

Figure S1 related to Figure 1. Comparison of primary and immortalized CPCs using data-independent acquisition mass spectrometry (DIA-MS). Analysis of differentially expressed proteins in samples collected after 28 days of chondrogenic differentiation. A total of 2449 proteins were detected. Cell lines were grouped together (group 1: CPC677 and CPC241hT; group 2: CPC674 and CPC674hT; group 3: CPC678 and CPC678hT). Venn diagram of (A) down- and (B) upregulated proteins after immortalization. (C) GO biological processes terms were significantly enriched in upregulated proteins of group 1 and downregulated proteins of group 3.

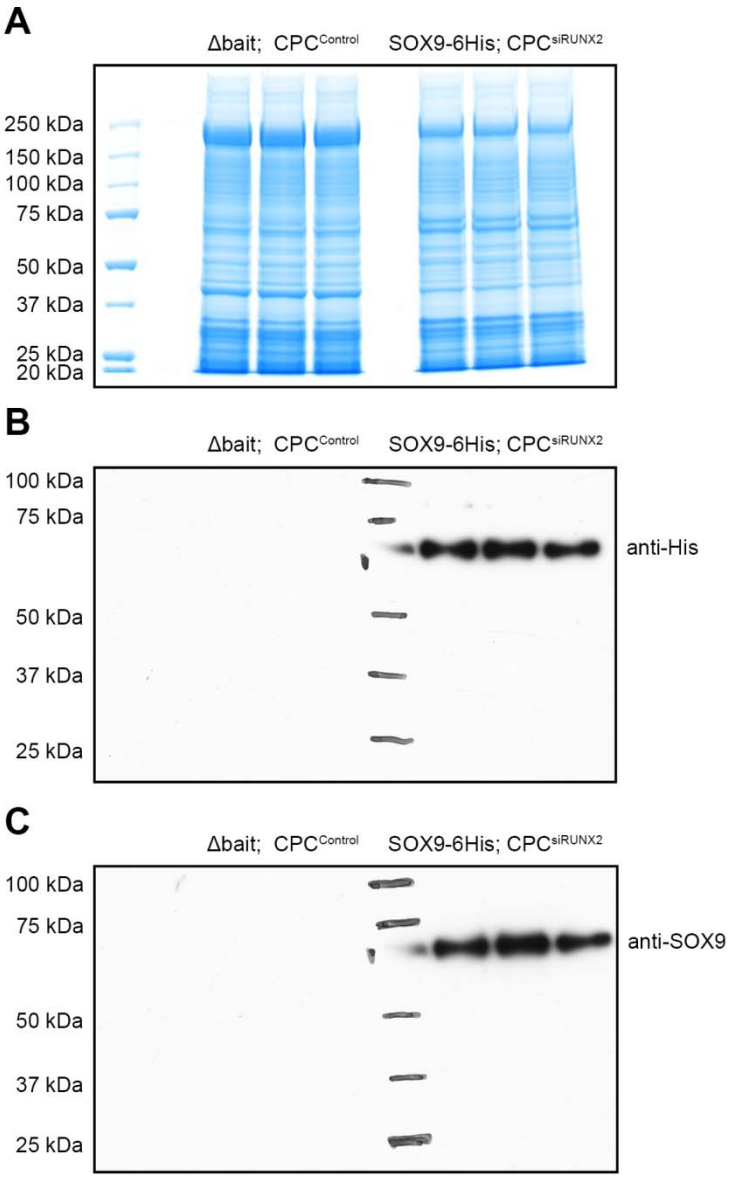

Figure S2 related to Figure 2. Full blot of CPC^{Control} and CPC^{siRUNX2} eluates after pulldown. Coomassie-stained SDS gel of CPC^{Control} and CPC^{siRUNX2} eluates (3 biological replicates respectively) after Δbait or SOX9-His pulldown. (B) Detection of His tag and (C) SOX9 by Western blotting.

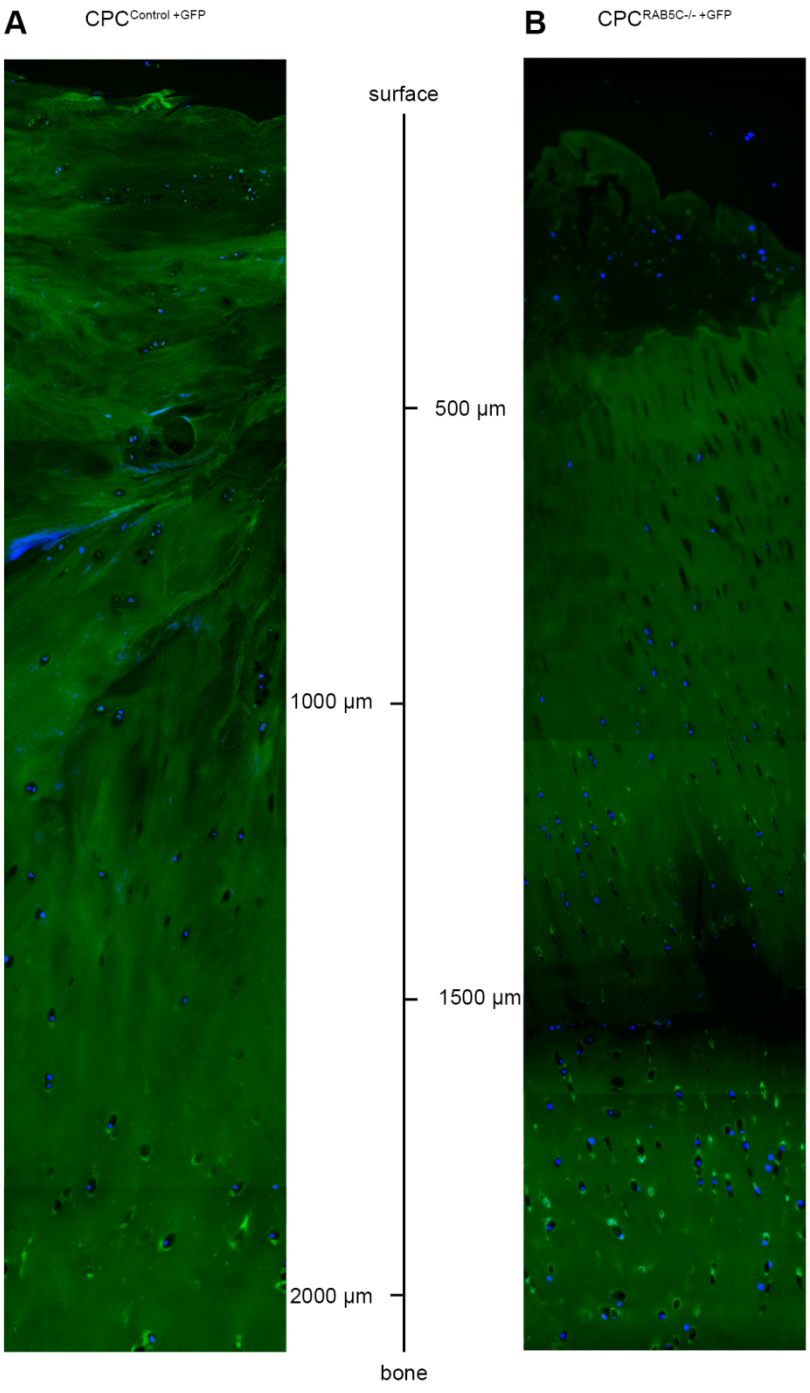

Figure S3 related to Figure 2. Ex vivo migration potential of CPC^{Control} and CPC$^{RAB5C-/-}$. GFP-transfected (A) CPC^{Control} and (B) CPC$^{RAB5C-/-}$ migrated to a depth of approximately 1800 µm deep in late-stage OA repair tissue samples after 4 days. Surface fissures were observed in all specimens. DAPI was used to stain the nuclei. The figure is assembled from individual images.

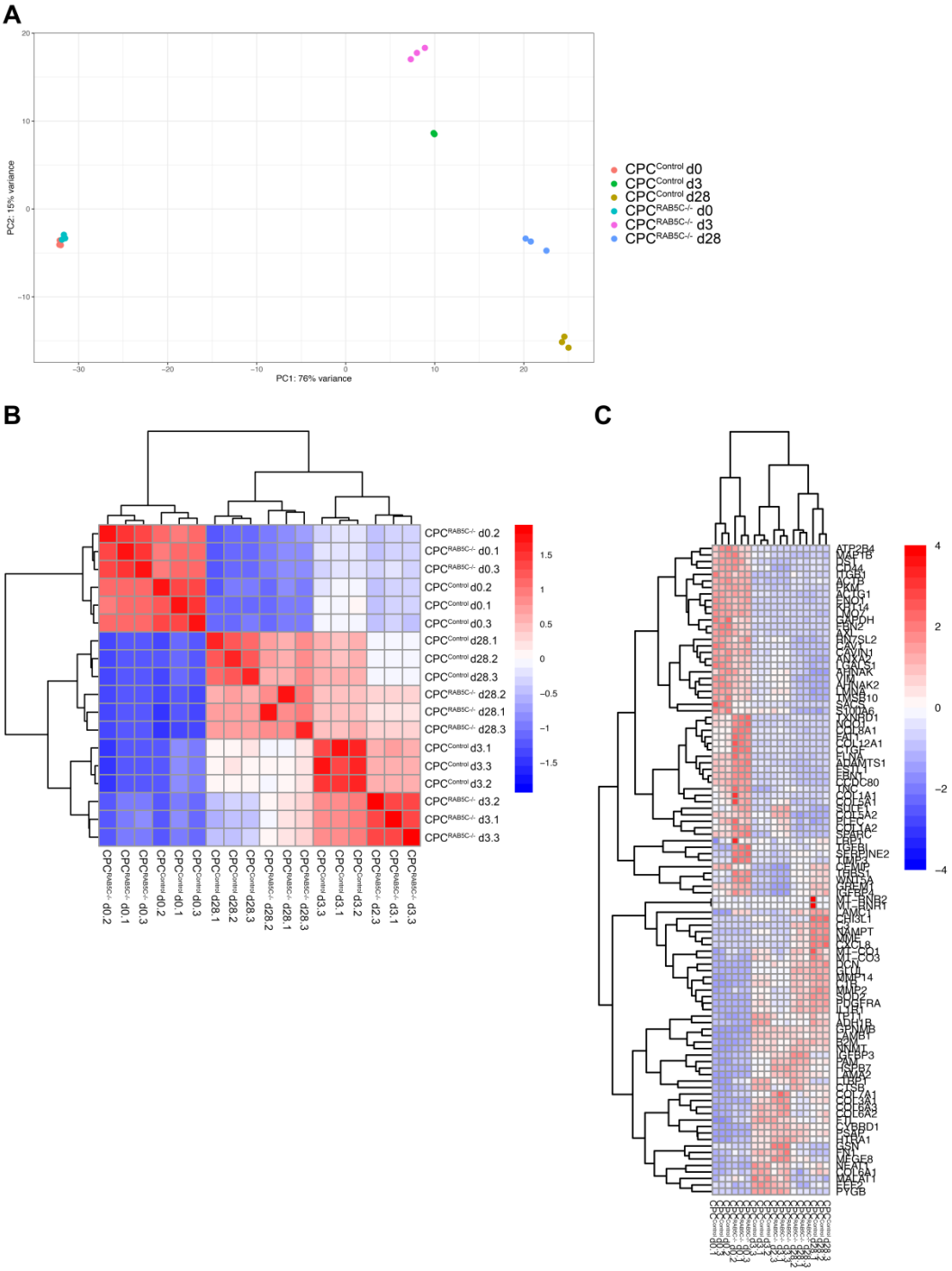

Figure S4 related to Figure 4. RAB5C-dependent gene expression during chondrogenic differentiation of CPCs. (A) Principal component analysis illustrating the clusters along the PC1 and PC2 coordinates during the time points investigated (d0, d3 and d28) and genotypes ($CPC^{Control}$ and $CPC^{RAB5C-/-}$) of CPCs. (B) Spearman correlation analysis of RNA-Seq biologically independent replicates.(C) Hierarchical clustering of the 100 most-variable genes during chondrogenic differentiation with individual samples.

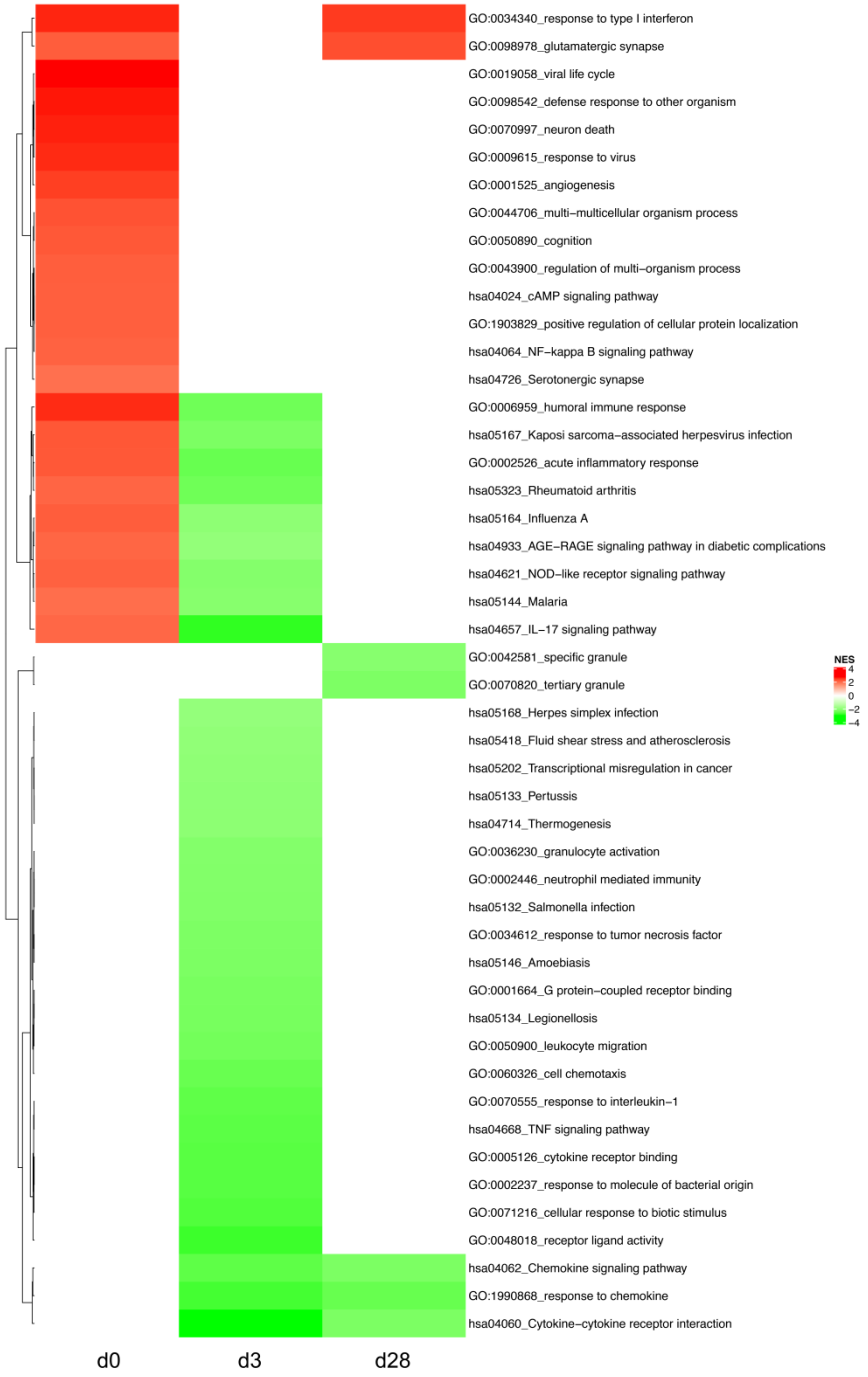

Figure S5 related to Figure 5. GSEA analysis of CPC$^{RAB5C-/-}$. Hierarchical clustering analysis of significantly enriched Gene Ontology (GO) terms and KEGG pathways for genes that were differentially expressed at days 0, 3 and 28 of chondrogenic differentiation between CPC^{Control} and CPC$^{RAB5C-/-}$ samples. Genes are derived from the RNA-Seq differential expression analysis and enrichment is calculated as the ratio of observed over expected genes and log2 fold change. The magnitude of deregulation in each term is displayed in colors ranging from green (downregulated) to red (upregulated).

Table S5. qPCR primers related to Figure 1.

Gene	Forward 5'-3'	Reverse 5'-3'
ACAN	GTGCCTATCAGGACAAGGTCT	GATGCCTTTCACCACGACTTC
BMPR1B	CTTTTGCGAAGTGCAGGAAAAT	TGTTGACTGAGTCTTCTGGACAA
COL1A1	TTCCCCCAGCCACAAAGAGTC	CGTCATCGCACAACACCT
COL1A2	CCTGGTGCTAAAGGAGAAAGAGG	ATCACCACGACTTCCAGCAGGA
COL2A1	TGGACGATCAGGCGAAACC	GCTGCGGATGCTCTCAATCT
COL9A2	CCTGGTGAGATTGGAATCCGAG	GAAATCCGCACTGCCTTCCAGA
COL11A1	ACCCTCGCATTGACCTTCC	TTTGTGCAAAATCCCGTTGTTT
GAPDH	GAAAAACCTGCCAAATATGATGA	ATTGTCATACCAGGAAATGAGCTT
IL4R	CGTGGTCAGTGCGGATAACTA	TGGTGTGAACTGTCAGGTTTC
NOTCH3	TACTGGTAGCCACTGTGAGCAG	CAGTTATCACCATTGTAGCCAGG
RAB5C	CATCAGCAAAGACTGCAATGA	GTTCTCCTGGAGGTCCACAC
RUNX2	TTCCAGACCAGCAGCACTC	CAGCGTCAACACCATCATT
SMAD7	TGTCCAGATGCTGTGCCTTCCT	CTCGTCTTCTCCTCCCAGTATG
SOX5	CTCGGCAAATGAAGGAGCAACTC	ACTGCCAGTTGCTGAGTCAGAC
SOX6	GCCTAAGTGACCGTTTTGGCAG	GGCATCTTTGCTCCAGGTGACA
SOX9	CAGGCTTTGCGATTTAAGGA	CCGTTTTAAGGCTCAAGGTG